

Alberta Wells Dataset: Pinpointing Oil and Gas Wells from Satellite Imagery

Pratinav Seth^{*12} Michelle Lin^{*13} Brefo Dwamena Yaw¹ Jade Boutot⁴ Mary Kang⁴ David Rolnick¹⁴³

Abstract

Millions of abandoned oil and gas wells are scattered across the world, leaching methane into the atmosphere and toxic compounds into the groundwater. Many of these locations are unknown, preventing the wells from being plugged and their polluting effects averted. Remote sensing is a relatively unexplored tool for pinpointing abandoned wells at scale. We introduce the first large-scale Benchmark Dataset for this problem, leveraging high-resolution multi-spectral satellite imagery from Planet Labs. Our curated Dataset comprises over 213,000 wells (abandoned, suspended, and active) from Alberta, a region with especially high well density, sourced from the Alberta Energy Regulator and verified by domain experts. We evaluate baseline algorithms for well detection and segmentation, showing the promise of computer vision approaches but also significant room for improvement.

1. Introduction

Across the world, there are millions of abandoned oil and gas wells left to degrade by the companies or individuals that built them. No longer producing usable fossil fuels, these wells nonetheless have a significant impact on the environment, with many of them leaking significant quantities of methane, a powerful greenhouse gas, into the atmosphere. In aggregate, these emissions represent the equivalent of millions of tons of carbon dioxide per year (Williams et al., 2020). In Canada, an estimated 370,000 abandoned wells produce methane equivalent to half a million metric tons of CO₂ annually (Williams et al., 2020; ECCC, 2024), while in the U.S., there are an estimated 4 million abandoned

wells (Williams et al., 2020), releasing over five million metric tons of CO₂ equivalent emissions per year. Despite the small percentage, the high global warming potential of methane underscores the need for improved monitoring and management to reduce environmental impact. Abandoned wells also pose health and safety concerns, in particular by leaching toxic chemicals into the groundwater of surrounding communities (Cahill et al., 2019). It is possible to plug abandoned wells to mitigate the harms associated with them (with so-called “super-emitter” wells an especially high priority (Riddick et al., 2024; Kang et al., 2016)). However, a significant fraction of abandoned wells remain unknown. In Pennsylvania, as much as 90% of abandoned wells are estimated to be unrecorded (Kang et al., 2016). In Canada, abandoned wells have been described as the most uncertain source of methane emissions nationally due to the poor quality of data surrounding them (Williams et al., 2020).

With the advent of large-scale remote sensing datasets and powerful machine learning tools to process them, it has become possible to label and monitor the built environment as never before (Rolf et al., 2024). Many such works have focused on opportunities to use remote sensing to accelerate climate action and environmental protection, and oil and gas infrastructure has increasingly been an object of scrutiny (see e.g. Yang et al. (2013); Sheng et al. (2020)). In this work, we present the first large-scale machine-learning benchmark dataset for pinpointing onshore oil and gas wells, encompassing abandoned, suspended, and active wells. Our main contributions are as follows:

- We introduce the Alberta Wells Dataset, containing information on over 200k abandoned, suspended, and active onshore oil and gas wells with high-resolution satellite imagery. Our Dataset available at: <https://zenodo.org/records/13743323>.
- We frame the problem of identification of wells as a challenge for object detection and binary segmentation.
- We evaluate a wide range of state-of-the-art deep learning algorithms, showing promising performance but emphasizing the challenging nature of the task.

We hope that this work will represent a step towards scalable identification of abandoned well sites and the reduction of their deleterious effects on our climate and environment.

^{*}Equal contribution ¹Mila Quebec AI Institute, Montreal, Canada ²Department of Data Science & Computer Application, Manipal Institute of Technology, Manipal Academy of Higher Education, Manipal, Karnataka, India ³Université de Montréal, Montreal, Canada ⁴McGill University, Montreal, Canada. Correspondence to: Pratinav Seth <seth.pratinav@gmail.com>.

Table 1. Previous datasets in which remote sensing algorithms are applied to detect oil and gas wells. “N/A” is given for datasets that do not indicate the number of individual wells in the dataset.

Dataset	O&G Well Count	Total Well Images	Resolution (m/px)	Geography	Imagery Source
NEPU-OWOD V1.0 (Wang et al., 2021)	1,192	432	0.41	Daqing City, China	
NEPU-OWOD V3.0 (Zhang et al., 2023)	3,749	722	0.48	China & California	
Oil Well Dataset (Shi et al., 2021)	N/A	5,895	0.26	Daqing City, China	
O&G Infrastructure (Guisiano et al., 2024)	630	930	0.15 - 1	Permian Basin, USA	
Well Pad Dataset (Ramachandran et al., 2024)	12,490	10,432	0.3-0.7	Permian and Denver Basins, USA	Google Earth
NEPU-OWS V1.0 (Wu et al., 2023b)	N/A	1,200	10	Russia	
NEPU-OWSV2.0 (Wu et al., 2023a)	N/A	120	10/20/60	Austin, USA	Sentinel-2
Alberta Well Dataset (Ours)	213,447	94,343	3	Alberta, Canada	Planet Labs

2. Previous Work

Hundreds of satellites continuously monitor the Earth’s surface, generating petabyte-scale remote sensing datasets (Rolf et al., 2024). With advancements in hardware, the quality of remote sensing images has significantly improved in terms of spatial and temporal resolution. High-quality remote sensing data are available through state-funded projects like Sentinel and Landsat and, more recently, through private enterprises such as Planet Labs (PBC, 2024). Increasingly, machine learning has been used to parse such raw data, including in various applications for tackling climate change (Yang et al., 2013). Benchmark datasets in this area have included tasks in land use and land cover (LULC) estimation (Sumbul et al., 2019), crop classification (Tseng et al., 2021), and forest monitoring (Bountos et al., 2025). Although developed primarily for urban monitoring, the SpaceNet 7 dataset (Van Etten et al., 2021) features a small number of study sites with oil wells.

Within this area of research, an increasing body of work has considered the problem of detecting artifacts associated with oil and gas operations. The detection of oil spills using a combination of remote sensing and machine learning has been widely explored (Wang et al., 2023a; Yang et al., 2022). Recently, the detection of oil and gas infrastructure has also been investigated (Prajapati et al., 2022), with some studies focusing on the goal of estimating methane emissions (Zhu et al., 2022; Omara et al., 2023). The dataset by Sheng et al. (2020) includes 7,066 aerial images, with 149 images of oil refineries. The METER-ML dataset (Zhu et al., 2022) comprises 86,599 georeferenced images in the U.S. labeled for methane sources. The OGIM v1 dataset (Omara et al., 2023) includes 2.6 million point locations of major facilities. A dataset by Chang et al. (2023) features 1,388 images of pipelines in the Arctic, while a dataset by Wang et al. (2023b) includes 3,266 images of heavy-polluting enterprises with 0.25 m resolution.

The problem of detection of oil and gas wells has also been proposed by a number of authors. However, Existing datasets are quite small (500-10,000) and typically are limited to a small region and contain only active wells, limiting

Table 2. Statistics of instances and wells across the dataset.

Split	Total Patches	Wells/ Non-Wells Patches	Count of Well Type in Wells Patches of Split		
			Abandoned	Suspended	Active
Train	167436	83718	46342	47595	100294
Validation	9463	4731	3166	2671	2406
Test	11789	5894	4024	3609	3340

their applicability in identifying abandoned or suspended wells as summarized in Table 1. Most of these studies have primarily focused on basic machine learning algorithms for well detection due to the limited sample size.

3. Alberta Wells Dataset

We introduce the Alberta Wells Dataset for oil and gas well detection. The dataset is drawn from the province of Alberta, Canada, a region with the third-largest oil reserves in the world and a substantial number of oil and gas wells, many of which have been present for over a century. The entire province of Alberta (an area larger than the UK and Germany combined) encompasses a diverse range of geographical zones and is highly diverse for a landlocked region, including prairies, lakes, forests, and mountains. The dataset contains over 188,000 patches of satellite imagery acquired by Planet Labs (PBC, 2024), which we make publicly available, with around 94,000 containing wells covering more than 213,000 individual wells. (More Details in Table 2). Each patch is annotated with labels for both segmentation and bounding box localization. The annotations are based on data from the Alberta Energy Regulator (AER, 2024), quality-controlled by domain experts.

Our dataset attempts to maximize the amount of data available for learning by including a mixture of active and suspended wells alongside abandoned wells. These types of wells appear overall similar in satellite imagery. In contrast to abandoned wells, “suspended” refers to wells that have merely paused operations temporarily, though this designation can be inaccurate, and some wells are classified as suspended for long enough that they are truly abandoned. Active wells are those that are currently in operation.

To simulate real-world conditions, we ensure a varied den-

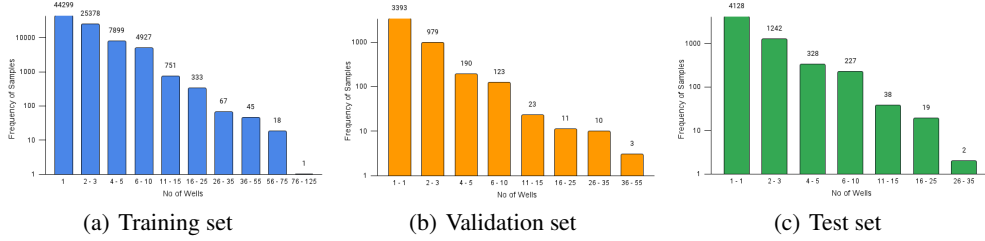


Figure 1. Distribution of the number of individual wells in positive samples from the dataset. We also include an equal number of images with no wells at all.

Table 3. Information on the numbers of wells represented in the dataset across different states (suspended, abandoned, and active). It also includes domain-specific metadata, such as the mode of operation and the types of fossil fuels extracted, which were used for filtering and quality control.

Well State	Count	License Status	Mode Short Description	Fluid Short Description
Suspended	55007	Suspension	All	Gas, Crude oil, Crude bitumen, Liquid petroleum gas, Coalbed methane-coals and other Lith, Coalbed methane-coals only, Shale gas only, Acid gas, CBM and shale and other sources, Shale gas and other sources.
		Issued	Suspended	
		Amended		
Abandoned	54947	Abandoned	All	Gas, Crude oil, Crude bitumen, Liquid petroleum gas, Coalbed methane-coals and other Lith, Coalbed methane-coals only, Shale gas only, Acid gas, CBM and shale and other sources, Shale gas and other sources.
		Issued	Abandoned, Abandoned Zone, Junked and Abandoned.	
		Amended		
Active	107139	Issued	Flowing, Pumping, Gas Lift.	Gas, Crude oil, Crude bitumen, Liquid petroleum gas, Coalbed methane-coals and other Lith, Coalbed methane-coals only, Shale gas only, Acid gas, CBM and shale and other sources, Shale gas and other sources.
		Amended	Abandoned and Re-Entered	
		Re-Entered		

sity of wells per image, as highlighted in Figure 1. We also include satellite imagery patches with no wells present from areas nearby to areas with wells, ensuring no overlap between the samples. This balanced dataset maintains an equal distribution of well and non-well images. Table 2 details the total sample count in each dataset split.

3.1. Data Collection, Quality Control & Patch Creation

The Alberta Energy Regulator (AER) oversees the energy industry in the province, ensuring companies adhere to regulations as they develop oil and gas resources. AER publishes AER ST37 (AER, 2024), a monthly list of all wells reported in Alberta, detailing their geographic location, mode of operation, license status, and type of product being extracted, among other attributes. This data provides a metadata (.txt) file and a .shp shape file, where each entry represents a unique geo-location point per site but often contains duplicates. However, this data cannot be used directly because the license status or mode of operation does not always correlate with the actual status of the well and often contains duplicates. Therefore, we work with domain experts to perform quality control as illustrated in Figure 5 (Appendix).

First, we remove duplicate entries from the well metadata, which often contain multiple instances of the same well identified by duplicate license numbers. We resolve these duplicates by retaining the most recent update. A similar approach is applied to the shapefile, where duplicates are resolved using the license date. Afterward, we merge both datasets and filter the data, categorizing the wells as active,

abandoned, or suspended based on criteria developed in consultation with domain experts, as shown in Table 3. We check for duplicate location coordinates in the dataset and resolve them by retaining the instance with the latest drill date. Finally, we ensure all the well instances in the dataset are within Alberta’s boundaries. The raw metadata file has around 637,000 instances, while the surface hole geometry file has around 512,000 instances. After filtering and performing quality control on the datasets with domain experts, we have around 217,000 instances. We then calculate the geographical bounds covered by the well instances across the province and divide the region into non-overlapping square image patches, each covering an area of 1.1025 sq km (with sides of 1050m). These images include various numbers of individual wells (see Figure 1), and we ensure that an approximately equal number of patches exist with and without wells. As a result of this process, some samples were excluded due to being located outside Alberta’s geographical boundaries, leading to a final total of approximately 213,000 well instances in the dataset patches.

3.2. Dataset Splitting

To create a well-distributed dataset that represents various geographical regions and offers a diverse dataset for evaluation, we developed a splitting algorithm (Algorithm 1) which focuses on balancing regions, not individual examples, ensuring that both the training and test sets reflect a diverse range of regions from Alberta’s varied landscape. This approach preserves dataset diversity and simulates real-world conditions where imbalances are common.

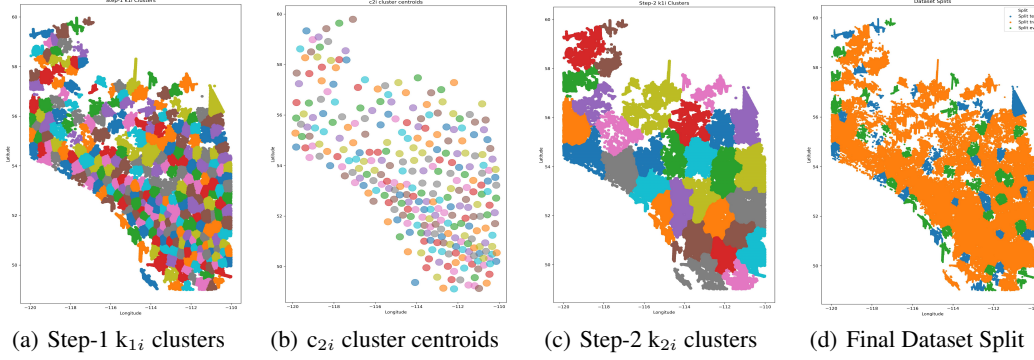


Figure 2. Illustration of the outcome of applying our dataset splitting algorithm: In Figures (a) to (c), different colors represent various cluster IDs. In Figure (d), blue refers to the training set, orange to the validation set, and green to the test set.

Algorithm 1 Clustering Algorithm for Dataset Splitting

W : Set of image patches ids containing wells; NW : Set of image patches ids not containing wells

Input: x_i represents the i -th patch with centroid coordinates c_i , where $i \in W$ or $i \in NW$;

Output: T_s : Test Set; T_r : Train Set; E_v : Eval Set;

Step 1: Clustering into M Clusters

Perform K-Means Clustering $k_1(*)$ with M clusters using all centroid coordinates c_i , where $i \in W$.

Assign each i -th patch into the m -th cluster where $m \in \{1, \dots, M\}$ and $i \in W$: cluster $k_{1i} = k_1(c_i) = m$ and update patches (x_i, c_i, k_{1i})

for $z \in \{1, \dots, M\}$ **do**

$W_{cz} = \{j \in W \mid k_{1j} = z\}$

Calculate cluster centroids c_{2j} based on values of c_i and update patch: $(x_i, c_i, k_{1i}, c_{2j})$, where $i \in W_{cz}$.

end for

Step 2: Clustering into N Super Clusters

Let W_{cc} be the set of unique c_{2j} for $j \in W$

Perform K-Means clustering $k_2(*)$ with N clusters using all $c_{2i} \in W_{cc}$.

Assign each $c_{2i} \in W_{cc}$ to n -th cluster, where $n \in \{1, \dots, N\}$ & $k_{2i} = k_2(c_{2i}) = n$.

Update patches $(x_j, c_j, k_{1j}, c_{2j}, k_{2j})$ where $c_{2j} = c_{2i}$ and $j \in W$.

Step 3: Assigning Patches to Sets

for $z \in \{1, \dots, N\}$ **do**

Find all j with $k_{2j} = z$, where $j \in W$ as W_{fz} .

Find unique k_{1j} and count o_j associated with it for j in W_{fz} . The, assign k_{1j} with minimum counts as \min_1 and \min_2 .

For each i in W_{fz} , append i to E_v if $k_{1i} = \min_1$, to T_s if $k_{1i} = \min_2$, otherwise to T_r .

end for

Step 4: Assigning Non-Well Patches

for each set_counter in $\{E_v, T_s, T_r\}$ **do**

for each unique k_{1i} as $z_i \in \text{set_counter}$ **do**

Find convex hull radius $r(z_i)$ of area occupied by c_j , where $j \in \text{set_counter}$ & $k_{1j} = z_i$.

Locate non-well patches $f \in NW$ within radius $r(z_i)$ not in any other cluster; Assign f to cluster z_i : (x_f, c_f, k_{1f}) : $k_{1f} = z_i$.

end for

end for

Step 5: Imbalance Correction

T_w refers to Count of Well Instances & T_{nw} refers to Count of Non-Well Instances in a Dataset Split

if $T_{nw} \neq T_w$ **then**

Identify clusters k_{1j} in data split contributing to the imbalance of excess non-well patches, assign to W_{ic}

for each i in W_{ic} **do**

$R(i) = (T_{nw} - T_w) \cdot \frac{\text{Count_Non_Wells}(k_{1i})}{\sum \text{Count_Non_Wells}(k_{1l}) \text{ where } l \in W_{ic}}$; where $R(i)$ is the no. of Samples to be Removed from i -th Cluster.

end for

else

Sample non-well patches x_j : $j \in NW$ & $j \notin k_{1j}$.

end if

This method involves forming small clusters k_{1i} of nearby well patches based on their centroids as illustrated in Figure 2 (a). These small clusters are then grouped into larger, non-intersecting super-clusters k_{2i} , with each super-cluster representing a city or larger geographical area. The formation of super-clusters involves calculating a centroid for each k_{1i} cluster based on the centroids of the well patches it contains as illustrated in Figure 2 (b). By clustering wells in this manner, we ensure that k_{1i} clusters group wells from nearby localities together, while k_{2i} clusters group wells from the same geographic region as illustrated in Figure 2 (c). Thus, each k_{2i} cluster represents a geographic distribution, with each k_{1i} cluster within it representing a sample of that distribution. To ensure a diverse and well-distributed evaluation and testing of our machine learning model, we select the k_{1i} clusters with the two fewest well instances from each k_{2i} super-cluster for inclusion in the evaluation and test sets. This approach ensures a diverse representation of the dataset as observed in Figure 2 (d). Moreover, we maintain an equal distribution of well and non-well patches. In cases of imbalance in non-well images, we exclude such patches from the contributing k_{1i} clusters as specified in Algorithm 1. For imbalances in well images, we sample non-well patches that are not part of any other clusters.

The parameters used in constructing the dataset are $M = 300$ and $N = 30$. These were picked heuristically so as to create a well-distributed dataset. Alberta's varied landscape offers a rich environment for creating a comprehensive oil well dataset. Training machine learning models on this extensive dataset improves their robustness and ability to generalize to similar, less-studied regions, thereby supporting well detection and efforts to mitigate global warming. By forming non-overlapping clusters (k_{1i}), each with its own well and non-well patches, we minimize the risk of data leakage while ensuring diversity. We also balanced non-well images across clusters to better simulate real-world conditions and maintain the diversity of the dataset.

3.3. Satellite Imagery Acquisition & Label Creation

We used PlanetScope-4-Band imagery (PBC, 2024) featuring RGB and Near Infrared bands to represent satellite images of the region with a medium resolution of about 3 meters per pixel. PlanetScope, a product of Planet Labs, consists of approximately 130 satellites that can image the entire Earth’s land surface daily, collecting up to 200 million sq. km of data each day. We obtained Surface Reflectance imagery, which is offset-corrected, flat-field-corrected, ortho-rectified, visually processed, and radiometrically corrected. These processes ensure consistency across varying atmospheric conditions and minimize uncertainty in spectral response over time and location, making the data ideal for various applications.

We choose Planet Labs data over other alternatives since it is updated daily, making it possible to pick a consistent time for all the images, which is important for training dataset consistency. It also provides multispectral imagery (4-band: RGB+Near Infrared), and the Near Infrared band is a useful addition (as we later verify in Table 7) since certain features, like ground depressions indicating well sites, may be more detectable in this band. Lastly, while other alternatives may be limited in remote regions, Planet’s global satellite constellation ensures more consistent coverage. All the imagery we use is made publicly available in the dataset. To ensure the highest quality, we selected images with no cloud cover. The images were acquired by Planet satellites within a timeframe that aligns with the well-location data from AER. We obtained satellite images for each sample based on geographical coordinates, ensuring an intersection between the actual area of interest and the acquired imagery.

We frame the task of identifying wells as both an object detection and segmentation task. In a real-world setting, high performance in either detection or segmentation would be sufficient for detection of wells; therefore we test both framings since it is not *a priori* clear which may be best suited to remote sensing algorithms. For each image patch, as shown in Figure 3, we generated corresponding segmentation maps and object detection annotations for all known wells in the image based on the point labels provided in the AER data. For binary segmentation, we annotated each well site with a circle to match the teardrop shape typical for well sites. We standardized the diameter of a well site to a value of 90 meters (such sites typically range from 70 to 120 meters in diameter). We used the same scale to define bounding boxes in the object detection task, following the COCO (Lin et al., 2014) format for annotations. The overlap in ground truth bounding boxes for some of the wells in Figures 3, 4, 10 and 11 reflects the clustering of multiple wells in densely developed oil and gas sites, where the spatial overlap of wells and infrastructure is common. (Note that this is a characteristic of the data, not a limitation of our quality control

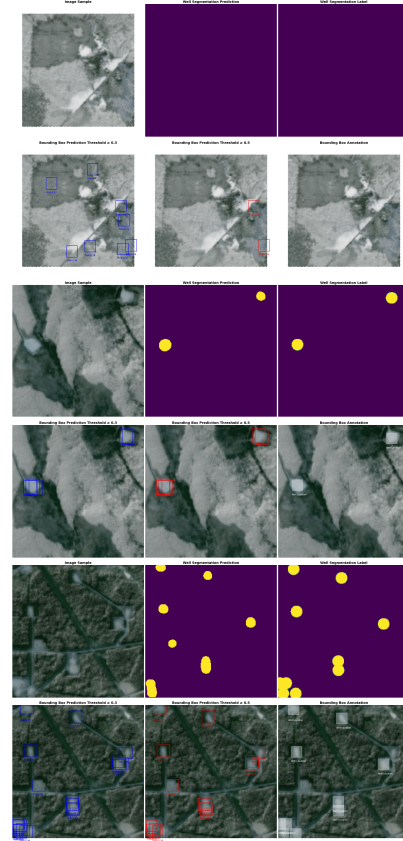


Figure 3. Sample image patches from our dataset includes examples with no wells, two wells, and multiple wells. Additionally, we present qualitative results with predictions generated by our Segmentation U-Net (ResNet50) and DETR ResNet50 model.

strategy.) Additionally, we created multi-class segmentation maps, where each class represents a different state of the well (active, suspended, or abandoned), and included this information in the object detection annotations. (We do not perform multi-class segmentation experiments here, but it is possible that future researchers may find this task useful.)

4. Experiments

We evaluate the performance of deep learning models for binary segmentation and object detection tasks. Our focus includes all oil and gas wells, regardless of their operational status, since they exhibit similar footprints and consistent features, making them detectable in satellite imagery.

We augment images by randomly resizing images to 256×256 , ensuring all bounding boxes remain intact for object detection. We then apply horizontal and vertical flipping with a probability of 0.25 each, followed by normalization using channel-wise mean and standard deviation calculated from the training split of the dataset. The hyperparameters we use in these various models represent standard perfor-

mant settings and are not intended to represent the outcome of hyperparameter optimization.

4.1. Binary Segmentation

We selected well-known baseline models for binary segmentation, encompassing the deep CNN-based approaches U-Net, PAN, and DeepLabV3+, as well as the Transformer-based architectures Segformer and UperNet.

U-Net (Ronneberger et al., 2015) was chosen for its widespread use as a baseline, offering an effective encoder-decoder architecture for multi-scale feature extraction. PAN (Li et al., 2018) improves multi-scale context with pyramid pooling and attention mechanisms. DeepLabV3+ (Chen et al., 2018) was selected for its popularity in remote sensing tasks with its Atrous Convolution and ASPP module for capturing contextual information at various scales. SegFormer (Xie et al., 2021) is a transformer-based architecture designed for semantic segmentation, utilizing self-attention mechanisms for capturing long-range dependencies. UperNet (Xiao et al., 2018) combines UNet and PSPNet (Zhao et al., 2017) architectures, featuring a UNet-like structure for multi-scale feature fusion and PSPNet’s pyramid pooling module integrated with a Swin Transformer (Liu et al., 2021) backbone for efficient multi-scale processing.

We train all CNN-based models using a ResNet50 backbone, a batch size of 128, and the BCELogits loss function. To fine-tune the model, a cosine annealing scheduler (Loshchilov & Hutter, 2017) is used, which adjusts the learning rate smoothly in a cyclical manner by gradually decreasing it. We also experimented with additional backbones with U-Net to evaluate the impact of backbones with larger receptive fields and attention mechanisms. This included ResNeXt50 (Xie et al., 2017), which enhances feature learning through grouped convolutions; SE-ResNet50 (Hu et al., 2018), which introduces channel-wise attention with Squeeze-and-Excitation blocks; and EfficientNetB6 (Tan & Le, 2019), known for its balanced scaling. In segmentation, the combination of UperNet’s contextual aggregation and the ConvNeXt backbone’s efficient representation enables precise segmentation, particularly valuable for remote sensing applications. For transformer-based models, while both Segformer and UperNet use a Dice loss function and a polynomial learning rate scheduler, Segformer utilizes a mit-b0-ade (Xie et al., 2021) backbone with a batch size of 128, while UperNet uses ConvNeXT (small and base) and Swin Transformer backbones with a batch size of 64. All models are optimized using AdamW for 50 epochs.

We evaluate the binary segmentation task with respect to IoU, Precision, Recall, and F1-Score. High Precision corresponds to reducing false positives, while high Recall corresponds to reducing false negatives. IoU measures the overlap between predicted and ground truth masks, offering

further insight into segmentation accuracy. F1-Score, the harmonic mean of precision and recall, provides a balanced measure considering both false positives and false negatives.

4.2. Object Detection

For binary object detection, we consider both single-stage, i.e., RetinaNet (Lin et al., 2017), FCOS and SSD, and two-stage CNN-based architectures, i.e. Faster R-CNN (Ren et al., 2017), and the transformer-based architecture DETR (Carion et al., 2020). RetinaNet (Lin et al., 2017) is a one-stage architecture trained using focal loss, which helps to address class imbalance. It uses a Feature Pyramid Network for multi-scale feature extraction and efficient object detection across different scales. Faster R-CNN (Ren et al., 2017) is a two-stage model recognized for its high accuracy. It employs a Region Proposal Network for generating region proposals and a separate network for predicting class labels and refining bounding box coordinates. FCOS (Fully Convolutional One-Stage Object Detection) (Tian et al., 2019) directly predicts object locations and categories from feature maps, which is effective for small object detection. SSD (Single Shot MultiBox Detector) (Liu et al., 2016) uses multiple feature maps at different scales, enhancing its accuracy for small objects. DETR (DEtection TRansformers) is a transformer-based model that treats object detection as a set prediction problem. It eliminates the need for specialized components such as anchor boxes and NMS, using transformers to directly predict the final set of detections.

All object detection models are trained using a ResNet50 backbone, except for SSD Lite, which is trained with a MobileNet backbone. The batch size is set to 256 for Faster R-CNN and FCOS and 512 for RetinaNet and SSD Lite. We used a cosine annealing scheduler (Loshchilov & Hutter, 2017) and trained all models for 120 epochs. DETR similarly uses a ResNet50 backbone but has a batch size set to 64. All models are optimized using the AdamW optimizer. For binary object detection model evaluation, we calculate Intersection over Union (IoU) at various thresholds (e.g., $\text{IoU}_{0.1}$, $\text{IoU}_{0.3}$, $\text{IoU}_{0.5}$), which measures how well predicted bounding boxes align with ground truth. IoU is computed by dividing the area of overlap by the area of their union, with higher values indicating better alignment. IoU thresholds define the minimum overlap required for a predicted box to match a ground truth box. (For example, an $\text{IoU}_{0.5}$ threshold means a predicted box must have at least 50% overlap with a ground truth box to be considered a correct detection.) We also assess Mean Average Precision (mAP), including mAP_{50} and $\text{mAP}_{50:95}$, measuring the model’s precision-recall trade-off and detection accuracy at various IoU thresholds. mAP_{50} measures precision at an IoU threshold of 0.5, while $\text{mAP}_{50:95}$ averages precision across IoU thresholds from 0.5 to 0.95. Higher mAP scores reflect better detection accuracy and precision. While higher IoU

Table 4. Results for the binary segmentation task for a variety of models evaluated over the test set. We report the Intersection over Union (IoU), precision, recall, and F1-score.

Architecture	Backbone	Params	GFLOPs	IoU	F1 Score	Precision	Recall
U-Net	ResNet50	32.52M	21.42	58±0.5	61.9±0.8	90.2±2.2	62.3±1.6
	ResNext50	32M	21.81	58.2±0.2	62.1±0.3	88.2±3.5	63.6±1.7
	SE_ResNet50	35.06M	20.83	58.9±0.7	62.9±0.7	88.8±1.6	64.4±1.4
	EfficientNetB6	43.83M	-	60.4±0.3	64.8±0.4	87.8±0.4	66.3±0.3
PAN	ResNet50	24.26M	17.47	57.8±0.8	61.5±0.9	89.3±1.2	61.5±0.9
DeepLabV3+	ResNet50	26.68M	18.44	56.8±0.7	60.6±0.7	89.4±1.3	61.8±1.1
Segformer	mit-b0-ade	3.72M	3.52	57.6±0.5	61.3±0.6	82.6±2.9	69.2±2.1
UperNet	ConvNexT-Small	128.29M	81.76	59.4±0.1	63.5±0.1	81.5±0.5	71.5±0.4
	ConvNexT-Base	146.27M	121.99	59.7±0.3	63.8±0.2	81.1±0.7	72.2±0.2
	swin small	81.15M	134.20	59.9±0.7	64.2±0.7	80.6±0.5	73.1±0.1

Table 5. Results for the object detection task for a variety of models evaluated over the test set. We report the intersection over union (IoU) over thresholds 0.1, 0.3, 0.5 and the mean average precision (mAP) for both IoU= 0.5 and IoU∈ [0.5, 0.95] thresholds.

Architecture	Backbone	Params	GFLOPs	IoU _{0.1}	IoU _{0.3}	IoU _{0.5}	mAP ₅₀	mAP _{50:95}
RetinaNet	ResNet50	18.87M	0.93	24.58±0.11	43.07±0.8	59.79±0.36	0.18±0.28	0.63±1.12
FasterRCNN		41.09M	24.7	36.79±1.07	46.95±0.66	61.29±0.35	5.20±1.00	19.12±3.41
FCOS		31.85M	25.81	34.79±0.99	48.51±0.59	62.66±0.43	9.67±1.47	30.46±3.11
SSD Lite	MobileNet	3.71M	0.64	33.91±0.18	50.30±0.08	65.07±0.03	9.76±0.39	25.14±0.66
DETR	ResNet-50	41.47M	6.86	41.78±0.11	51.15±0.14	63.17±0.11	15.22±0.28	38.45±0.32

values indicate better accuracy for individual predictions, mAP provides a broader measure of detection performance by capturing precision across different IoU criteria.

5. Results

Our tasks involve identifying a roughly circular well region with a 90m diameter in real life, which translates to less than 30 pixels in satellite imagery due to resizing and other augmentations. This poses a challenge for machine learning models given the heterogeneous nature of the background, including various similarly shaped and sized features of the natural and built environment. Additionally, vegetation can occlude wells in RGB channels, highlighting the importance of near-infrared imagery for guidance. The wells themselves also vary somewhat in shape and can be in various states of disrepair as a result of differing ages and maintenance.

5.1. Binary Segmentation

For the binary segmentation task framing, we train Models (from scratch) using both CNN-based and Transformer-based backbones, considering the prevalent imbalance in the image data due to the small size of wells. Although we did use 3-dimensional, ImageNet initialized weights of the backbone but modified the initial layers afterwards to support 4-dimensional multispectral images. Among our models, as shown in Table 4, the traditional U-Net with EfficientNetB6 backbone performs the best, with CNN-based models showing the highest IOU of 60.4 ± 0.3 and F1-Score of 64.8 ± 0.4 . While a ResNet50-based backbone achieves the highest Precision of 90.2 ± 2.2 , indicating more accurate predictions of well instances compared to other models. Precision, which reflects the accuracy of our positive detections compared to

the ground truth, is crucial. However, a high recall value ensures the model captures most actual well instances, reducing the risk of missing important information. Thus, the Uper-Net model with the highest recall value of 73.1 ± 0.1 , which excels at capturing global context information, appears a good candidate for this task, given a decent precision score. Taking into account both precision and recall, U-Net with EfficientNetB6 backbone performs well, suggesting the utility of a larger backbone with a bigger receptive field. However, ConvNexT Small provides a trade-off between computational efficiency and performance, requiring fewer GFLOPs and parameters compared to UperNet with Swin Small while achieving similar performance.

5.2. Binary Object Detection

Our evaluation, as shown in Table 5, indicates that while all models perform reasonably well in terms of aligning predicted and actual well locations, performance in the object detection task is overall lower than for segmentation – indicating that potentially segmentation is simply a better framing for this task in real-world settings. The observed gap in performance is likely attributed to the inherent challenge of detecting the small-sized wells within the satellite imagery. It is well-known that single-stage CNN architectures (such as FCOS and SSD) often demonstrate better performance on small object detection than two-stage methods (such as Faster R-CNN), and this aligns with our observations. The exception here is the single-stage method RetinaNet, which, although it has comparable IoU scores, struggles to detect wells accurately. SSD Lite stands out with the highest IoU_{0.5} score of 65.07 ± 0.03 and IoU_{0.3} score of 50.3 ± 0.08 . Whereas all models are quite similar in terms of IoU_{0.1}, the highest score by FasterRCNN is 36.79 ± 1.07 .

Table 6. Results for object detection task for the FCOS Model with ResNet50 backbone, trained with and without NIR Imagery.

Modality	IoU _{0.1}	IoU _{0.3}	IoU _{0.5}	mAP ₅₀	mAP _{50:95}
RGB+NIR	34.79±0.99	48.51±0.59	62.66±0.43	9.67±1.47	30.46±3.11
RGB	32.39±2.88	46.80±2.07	61.23±1.58	5.7±3.65	20.00±10.40

Table 7. Results for the binary segmentation task for U-Net with ResNet50 backbone, trained with and without NIR imagery.

Modality	IoU	F1 Score	Precision	Recall
RGB+NIR	58.00±0.50	61.9±0.80	90.20±2.20	62.30±1.60
RGB	56.60±0.44	60.50±0.35	87.00±1.40	62.54±0.13

Thus, SSD Lite and FCOS excel in localization, especially at higher IoU thresholds, while Faster R-CNN is adept at detecting objects with minimal overlap. All models demonstrate low performance in terms of mAP₅₀, which assesses precision-recall trade-off and detection accuracy at an IoU threshold of 0.5. FCOS achieves the of 9.67 ± 1.47 while SSD Lite achieves a score of 9.76 ± 0.39 . This may be due to these models not producing region proposals confidently enough, especially in instances with a large number of wells. Whereas over a broader evaluation with mAP_{50:95} which averages precision across IoU thresholds from 0.5 to 0.95. All models apart from RetinaNet provide much better results, with FCOS achieving the highest score of 30.46 ± 3.11 , indicating a decent performance in the identification of well instances. Most notably, the transformer-based model DETR demonstrates the strongest overall performance, achieving strong IoU scores across thresholds and the highest mAP50 (15.22 ± 0.28) and mAP50 : 95 (38.45 ± 0.32) scores. These results highlight DETR’s ability to effectively capture global contextual cues essential for accurate well detection.

5.3. Value Added from Dataset Breadth

In these experiments, we consider the value provided by our inclusion of (i) near-infrared (NIR) imagery in addition to RGB channels, and (ii) the inclusion of abandoned and suspended wells in addition to active wells.

Benefits of NIR imagery: We find that including the NIR band significantly enhances both object detection and segmentation performance compared to purely RGB data. In segmentation (Table 7), RGB+NIR outperforms RGB in IoU, F1 Score, and Precision while slightly lowering Recall. A similar trend is observed in the object detection (Table 6) with RGB+NIR achieves higher Intersection over Union (IoU) scores across all thresholds (0.1, 0.3, and 0.5) and a considerable increase in mAP@50 and mAP@50:95. These improvements can be attributed to the enhanced spectral information provided by the NIR band, which is particularly effective in detecting features such as ground depressions that may indicate well sites. These features are often more distinguishable in the NIR spectrum, leading to

Table 8. Performance comparison of U-Net with ResNet50 backbone for binary segmentation trained on active wells only versus all well types. Our results demonstrate that training merely on active wells is not sufficient to detect abandoned and suspended wells in practice – highlighting the importance of including all three types in the dataset.

Metric	Train Set (Well Type Label Present)	Test Set
IoU	Active (I)	0.502
	All (I+II+III)	0.576
F1 Score	Active (I)	0.503
	All (I+II+III)	0.614
Precision	Active (I)	0.998
	All (I+II+III)	0.913
Recall	Active (I)	0.502
	All (I+II+III)	0.614

better performance in both tasks.

Benefits of Using Multiple Well Types. While much past work has focused on active wells, we show that training on such data is insufficient to detect abandoned and suspended wells (which are often significantly harder to e.g. degradation and vegetation growth over time). The results in Table 8 show that including all well types significantly outperforms training on only active wells, improving IoU, F1 score, and recall. Recall in particular is key for monitoring, where missing abandoned wells is more important than erroneously flagging a location as a well.

6. Limitations

We do not envision any significant negative uses of our work. Localization of wells is primarily of interest to the climate change mitigation community and is not, for example, a primary means whereby fossil fuel companies select new locations for drilling. Therefore, we do not believe this dataset is susceptible to dual use risks.

One potential limitation of our work is that we rely on well locations listed by the Alberta Energy Regulator. It is likely that some true well locations are missing in this data, leading to the potential for false negatives in the ground-truth data for this problem. However, it is to be expected that this will not significantly affect the training of algorithms since these labels represent a small fraction of the negative locations in the dataset, and deep learning algorithms are known to be robust to moderate amounts of label noise (see e.g. Rolnick et al. (2017)). Instead the effect may simply be that the reported test accuracy is actually lower than the true value (due to certain correctly predicted well locations

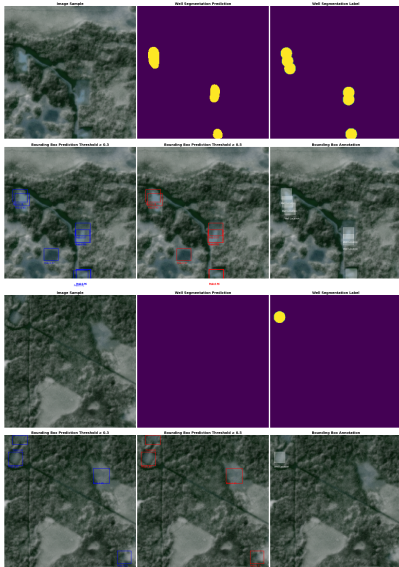


Figure 4. A few Sample image patches from our dataset presenting qualitative results with predictions of failure cases generated by our Segmentation U-Net and DETR with ResNet50 model.

being evaluated as false). We hope to investigate such effects further in future work.

Our dataset is focused on Alberta, because (1) it is a very large region with a significant amount of high-quality labeled data available, (2) it is one of the world’s most important locations for oil and gas production, so identifying wells in Alberta is of immediate impact. Future works may wish to assess the capacity for few- or zero-shot transfer learning from Alberta to other regions with a high expected concentration of abandoned wells, including the Appalachian and Mountain West regions of the United States, as well as a number of former Soviet states.

While our initial results offer encouragement, a deeper examination reveals a few failure cases arising from visually complex scenarios that highlight key challenges in our detection pipeline (as represented in Figure 4). Our model performs well in typical scenarios, where most patches contain only 1–5 wells. However, in rare high-density regions, performance can degrade — leading to undercounting or missed detections. Abandoned and suspended wells also pose a challenge due to their subtle visual signatures and minimal surface infrastructure. While near-infrared bands help in some cases, spectral cues alone are not always sufficient. Improving detection in these visually complex and low-signal cases is a key focus for future work.

7. Conclusion

In this paper, we present the first large-scale benchmark dataset aimed at identifying oil and gas wells, with a focus

on abandoned and suspended wells, which are a significant source of greenhouse gases and other pollutants. We combine high-resolution imagery, an extensive database of well locations, and expert verification to create the Alberta Wells Dataset. We frame well identification both in terms of object detection and binary segmentation and evaluate the performance of a wide range of popular deep learning methods on these tasks.

We find that the UperNet Model (with a ConvNexT backbone), in particular, represents the most promising baseline for the binary segmentation task, while for object detection, all models demonstrate more mixed results, with Single Stage Models (such as FCOS and SSD) providing a relatively promising baseline. These results show that the Alberta Wells Dataset represents both a challenging as well as a societally impactful set of tasks.

The value added by the dataset is twofold. First, most global fossil fuel-producing regions do not have databases of well locations comparable to that provided by AER. Alberta’s varied landscape provides an ideal setting for developing algorithms for the detection of wells, which can then be used directly in other locations or fine-tuned. Second, even in Alberta, the list developed by AER is not comprehensive, and many abandoned wells are believed to be missing; remote sensing algorithms can provide candidate locations for domain experts to examine so as to determine the true number and locations of abandoned wells in Alberta.

Overall, we hope that our work will make it possible to (i) better estimate the total effects of well-related methane emissions (currently extremely uncertain (Williams et al., 2020)) and groundwater contamination, (ii) prioritize wells to be plugged and decontaminated. We believe that the scalability of remote sensing will make it an invaluable tool in mitigating the global environmental impact of abandoned oil and gas wells.

Software and Data

Alberta Wells Dataset is available at: <https://zenodo.org/records/13743323>. Our Benchmarking Code is available at: https://github.com/RolnickLab/Alberta_Wells_Dataset.

Acknowledgments and Disclosure of Funding

This work was funded in part through the Canada CIFAR AI Chairs program and a McGill Tomlinson Scientist Award. We acknowledge support from Planet Labs in the form of their academic subscription program, and are grateful for the help of Tim Elrick in working with Planet data. We also thank Mila and the Digital Research Alliance of Canada for provision of computing facilities, and NVIDIA Corporation

for additional computational resources. Special thanks to Francis Pelletier, whose feedback on our data collection pipeline and coding significantly improved our methods.

Impact Statement

This work presents the first large-scale machine learning benchmark for pinpointing onshore oil and gas wells, including abandoned, suspended, and active wells. Our dataset, the Alberta Wells Dataset, contains over 200,000 well instances and high-resolution satellite imagery, enabling advancements in the identification of oil and gas wells. By framing the problem as one of object detection and binary segmentation, we hope this dataset will help improve the scalability and accuracy of well detection techniques.

Abandoned wells, particularly those that leak methane and other pollutants, pose a major environmental challenge. By improving methods for detecting these wells, this work aims to reduce their environmental impact by identifying high-emission sites that can be prioritized for remediation. This can contribute to mitigating climate change by helping to reduce harmful emissions from these otherwise difficult-to-detect sources.

To enable wider responsible uses of the dataset, we will release it under a non-commercial usage license, making it available for academic and research purposes only. We do not foresee significant negative impacts arising from this work. Dual uses of the algorithms we outline here are limited, and the algorithms used are comparatively small-scale and have low energy and carbon footprint.

References

- AER, A. E. R. ST37 — aer.ca. <https://www.aer.ca/providing-information/data-and-reports/statistical-reports/st37>, 2024. [Accessed 06-06-2024].
- Bountos, N. I., Ouaknine, A., Papoutsis, I., and Rolnick, D. Fomo: Multi-modal, multi-scale and multi-task remote sensing foundation models for forest monitoring, 2025. URL <https://arxiv.org/abs/2312.10114>.
- Cahill, A. G., Beckie, R., Ladd, B., Sandl, E., Goetz, M., Chao, J., Soares, J., Manning, C., Chopra, C., Finke, N., et al. Advancing knowledge of gas migration and fugitive gas from energy wells in northeast british columbia, canada. *Greenhouse Gases: Science and Technology*, 9 (2):134–151, 2019.
- Carion, N., Massa, F., Synnaeve, G., Usunier, N., Kirillov, A., and Zagoruyko, S. End-to-end object detection with transformers. In Vedaldi, A., Bischof, H., Brox, T., and Frahm, J.-M. (eds.), *Computer Vision – ECCV 2020*, pp. 213–229, Cham, 2020. Springer International Publishing. ISBN 978-3-030-58452-8.
- Chang, H., Bai, L., Wang, Z., Wang, M., Zhang, Y., Tao, J., and Chen, L. Detection of over-ground petroleum and gas pipelines from optical remote sensing images. In *Remote Sensing*, 2023.
- Chen, L.-C., Zhu, Y., Papandreou, G., Schroff, F., and Adam, H. Encoder-decoder with atrous separable convolution for semantic image segmentation. In *Proceedings of the European Conference on Computer Vision (ECCV)*, September 2018.
- ECCC. Greenhouse gas emissions. <https://www.canada.ca/en/environment-climate-change/services/environmental-indicators/greenhouse-gas-emissions.html>, 2024. [Accessed 28-09-2024].
- Guisiano, J. E., Moulines, É., Lauvaux, T., and Sublime, J. Oil and gas automatic infrastructure mapping: Leveraging high-resolution satellite imagery through fine-tuning of object detection models. In Luo, B., Cheng, L., Wu, Z.-G., Li, H., and Li, C. (eds.), *Neural Information Processing*, pp. 442–458, Singapore, 2024. Springer Nature Singapore. ISBN 978-981-99-8148-9.
- Hu, J., Shen, L., and Sun, G. Squeeze-and-excitation networks. In *2018 IEEE/CVF Conference on Computer Vision and Pattern Recognition*, pp. 7132–7141, 2018. doi: 10.1109/CVPR.2018.00745.
- Kang, M., Christian, S., Celia, M. A., Mauzerall, D. L., Bill, M., Miller, A. R., Chen, Y., Conrad, M. E., Darrah, T. H., and Jackson, R. B. Identification and characterization of high methane-emitting abandoned oil and gas wells. *Proceedings of the National Academy of Sciences*, 113 (48):13636–13641, 2016.
- Li, H., Xiong, P., An, J., and Wang, L. Pyramid attention network for semantic segmentation. In *British Machine Vision Conference 2018, BMVC 2018, Newcastle, UK, September 3-6, 2018*, pp. 285. BMVA Press, 2018. URL <http://bmvc2018.org/contents/papers/1120.pdf>.
- Lin, T.-Y., Maire, M., Belongie, S., Hays, J., Perona, P., Ramanan, D., Dollár, P., and Zitnick, C. L. Microsoft coco: Common objects in context. In Fleet, D., Pajdla, T., Schiele, B., and Tuytelaars, T. (eds.), *Computer Vision – ECCV 2014*, pp. 740–755, Cham, 2014. Springer International Publishing. ISBN 978-3-319-10602-1.
- Lin, T.-Y., Goyal, P., Girshick, R., He, K., and Dollár, P. Focal loss for dense object detection. In *2017 IEEE*

- International Conference on Computer Vision (ICCV)*, pp. 2999–3007, 2017. doi: 10.1109/ICCV.2017.324.
- Liu, W., Anguelov, D., Erhan, D., Szegedy, C., Reed, S., Fu, C.-Y., and Berg, A. C. Ssd: Single shot multibox detector. In Leibe, B., Matas, J., Sebe, N., and Welling, M. (eds.), *Computer Vision – ECCV 2016*, pp. 21–37, Cham, 2016. Springer International Publishing. ISBN 978-3-319-46448-0.
- Liu, Z., Lin, Y., Cao, Y., Hu, H., Wei, Y., Zhang, Z., Lin, S., and Guo, B. Swin transformer: Hierarchical vision transformer using shifted windows. In *2021 IEEE/CVF International Conference on Computer Vision (ICCV)*, pp. 9992–10002, 2021. doi: 10.1109/ICCV48922.2021.00986.
- Loshchilov, I. and Hutter, F. SGDR: Stochastic gradient descent with warm restarts. In *International Conference on Learning Representations*, 2017. URL <https://openreview.net/forum?id=Skq89Scxx>.
- Omara, M., Gautam, R., O’Brien, M. A., Himmelberger, A., Franco, A. P. B., Meisenhelder, K., Hauser, G., Lyon, D. R., Chulakadabba, A., Miller, C. C., Franklin, J. E., Wofsy, S. C., and Hamburg, S. P. Developing a spatially explicit global oil and gas infrastructure database for characterizing methane emission sources at high resolution. *Earth System Science Data*, 2023.
- PBC, P. L. Planet application program interface: In space for life on earth. <https://api.planet.com>, 2024.
- Prajapati, S., Raj, A., Chaudhari, Y., Nandwal, A., and Monga, J. S. OGInfra: Geolocating oil & gas infrastructure using remote sensing based active fire data. *ArXiv*, abs/2210.16924, 2022.
- Ramachandran, N., Irvin, J., Omara, M., Gautam, R., Meisenhelder, K., Rostami, E., Sheng, H., Ng, A. Y., and Jackson, R. B. Deep learning for detecting and characterizing oil and gas well pads in satellite imagery. *Nature Communications*, 15(1):7036, 2024.
- Ren, S., He, K., Girshick, R., and Sun, J. Faster r-cnn: Towards real-time object detection with region proposal networks. *IEEE Transactions on Pattern Analysis and Machine Intelligence*, 39(6):1137–1149, 2017. doi: 10.1109/TPAMI.2016.2577031.
- Riddick, S. N., Mbua, M., Santos, A., Emerson, E. W., Cheptonui, F., Houlihan, C., Hodshire, A. L., Anand, A., Hartzell, W., and Zimmerle, D. J. Methane emissions from abandoned oil and gas wells in colorado. *Science of The Total Environment*, 922:170990, 2024.
- Rolf, E., Klemmer, K., Robinson, C., and Kerner, H. Mission critical – satellite data is a distinct modality in machine learning. In *International Conference in Machine Learning (ICML)*, 2024.
- Rolnick, D., Veit, A., Belongie, S., and Shavit, N. Deep learning is robust to massive label noise. *arXiv preprint arXiv:1705.10694*, 2017.
- Ronneberger, O., Fischer, P., and Brox, T. U-net: Convolutional networks for biomedical image segmentation. In Navab, N., Hornegger, J., Wells, W. M., and Frangi, A. F. (eds.), *Medical Image Computing and Computer-Assisted Intervention – MICCAI 2015*, pp. 234–241, Cham, 2015. Springer International Publishing. ISBN 978-3-319-24574-4.
- Sheng, H., Irvin, J. A., Munukutla, S., Zhang, S., Cross, C., Story, K. T., Rustowicz, R., Elsworth, C. W., Yang, Z., Omara, M., Gautam, R., Jackson, R. B., and Ng, A. OGNet: Towards a global oil and gas infrastructure database using deep learning on remotely sensed imagery. *ArXiv*, abs/2011.07227, 2020. URL <https://api.semanticscholar.org/CorpusID:226964460>.
- Shi, P., Jiang, Q., Shi, C., Xi, J., Tao, G., Zhang, S., Zhang, Z., Liu, B., Gao, X., and Wu, Q. Oil well detection via large-scale and high-resolution remote sensing images based on improved YOLO v4. *Remote. Sens.*, 13:3243, 2021.
- Sumbul, G., Charfuelan, M., Demir, B., and Markl, V. Bigearthnet: A large-scale benchmark archive for remote sensing image understanding. In *IGARSS 2019 - 2019 IEEE International Geoscience and Remote Sensing Symposium*, pp. 5901–5904, 2019. doi: 10.1109/IGARSS.2019.8900532.
- Tan, M. and Le, Q. EfficientNet: Rethinking model scaling for convolutional neural networks. In Chaudhuri, K. and Salakhutdinov, R. (eds.), *Proceedings of the 36th International Conference on Machine Learning*, volume 97 of *Proceedings of Machine Learning Research*, pp. 6105–6114. PMLR, 09–15 Jun 2019. URL <https://proceedings.mlr.press/v97/tan19a.html>.
- Tian, Z., Shen, C., Chen, H., and He, T. Fcos: Fully convolutional one-stage object detection. In *2019 IEEE/CVF International Conference on Computer Vision (ICCV)*, pp. 9626–9635, 2019. doi: 10.1109/ICCV.2019.00972.
- Tseng, G., Zvonkov, I., Nakalembe, C. L., and Kerner, H. CropHarvest: A global dataset for crop-type classification. In *Conference on Neural Information Processing Systems (NeurIPS) Datasets and Benchmarks Track*, 2021.

- Van Etten, A., Hogan, D., Manso, J. M., Shermeyer, J., Weir, N., and Lewis, R. The multi-temporal urban development spacenet dataset. In *2021 IEEE/CVF Conference on Computer Vision and Pattern Recognition (CVPR)*, pp. 6394–6403, 2021. doi: 10.1109/CVPR46437.2021.00633.
- Wang, Y., Chen, X., and Wang, L. Cyber-physical oil spill monitoring and detection for offshore petroleum risk management service. *Scientific Reports*, 13, 2023a. URL <https://api.semanticscholar.org/CorpusID:257634108>.
- Wang, Z., Bai, L., Song, G., Zhang, J., Tao, J., Mulvenna, M. D., Bond, R. R., and Chen, L. An oil well dataset derived from satellite-based remote sensing. *Remote Sensing*, 13(6), 2021.
- Wang, Z., Zhao, X., Bai, L., Wang, M., Zhao, M., Fan, M., Tao, J., and Chen, L. Detection of heavy-polluting enterprises from optical satellite remote sensing images. In *IGARSS 2023 - 2023 IEEE International Geoscience and Remote Sensing Symposium*, pp. 6474–6477, 2023b.
- Williams, J. P., Regehr, A., and Kang, M. Methane emissions from abandoned oil and gas wells in Canada and the United States. *Environmental science & technology*, 55(1):563–570, 2020.
- Wu, H., Dong, H., Wang, Z., Bai, L., Huo, F., Tao, J., and Chen, L. Spatial information extraction of oil well sites based on medium-resolution satellite imagery. In *Image and Signal Processing for Remote Sensing XXIX*, volume 12733, pp. 127330K. International Society for Optics and Photonics, SPIE, 2023a.
- Wu, H., Dong, H., Wang, Z., Bai, L., Huo, F., Tao, J., and Chen, L. Semantic segmentation of oil well sites using Sentinel-2 imagery. In *IGARSS 2023 - 2023 IEEE International Geoscience and Remote Sensing Symposium*, pp. 6901–6904, 2023b.
- Xiao, T., Liu, Y., Zhou, B., Jiang, Y., and Sun, J. Unified perceptual parsing for scene understanding. In *Proceedings of the European Conference on Computer Vision (ECCV)*, September 2018.
- Xie, E., Wang, W., Yu, Z., Anandkumar, A., Alvarez, J. M., and Luo, P. Segformer: Simple and efficient design for semantic segmentation with transformers. In Ranzato, M., Beygelzimer, A., Dauphin, Y., Liang, P., and Vaughan, J. W. (eds.), *Advances in Neural Information Processing Systems*, volume 34, pp. 12077–12090. Curran Associates, Inc., 2021. URL https://proceedings.neurips.cc/paper_files/paper/2021/file/64f1f27bflb4ec22924fd0acb550c235-Paper.pdf.
- Xie, S., Girshick, R., Dollár, P., Tu, Z., and He, K. Aggregated residual transformations for deep neural networks. In *2017 IEEE Conference on Computer Vision and Pattern Recognition (CVPR)*, pp. 5987–5995, 2017. doi: 10.1109/CVPR.2017.634.
- Yang, J., Gong, P., Fu, R., Zhang, M., Chen, J., Liang, S., Xu, B., Shi, J., and Dickinson, R. The role of satellite remote sensing in climate change studies. *Nature Climate Change*, 3:875–883, 09 2013.
- Yang, J., Ma, Y., Hu, Y., Jiang, Z., Zhang, J., Wan, J., and Li, Z. Decision fusion of deep learning and shallow learning for marine oil spill detection. *Remote. Sens.*, 14:666, 2022.
- Zhang, Y., Bai, L., Wang, Z., Fan, M., Jurek-Loughrey, A., Zhang, Y., Zhang, Y., Zhao, M., and Chen, L. Oil well detection under occlusion in remote sensing images using the improved YOLOv5 model. *Remote Sensing*, 15(24), 2023.
- Zhao, H., Shi, J., Qi, X., Wang, X., and Jia, J. Pyramid scene parsing network. In *2017 IEEE Conference on Computer Vision and Pattern Recognition (CVPR)*, pp. 6230–6239, 2017. doi: 10.1109/CVPR.2017.660.
- Zhu, B., Lui, N., Irvin, J., Le, J., Tadwalkar, S., Wang, C., Ouyang, Z., Liu, F. Y., Ng, A. Y., and Jackson, R. B. METER-ML: A multi-sensor Earth observation benchmark for automated methane source mapping, 2022.

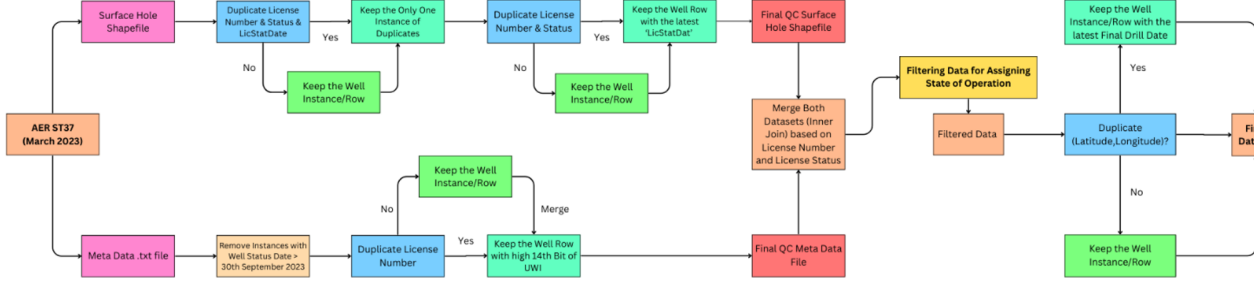


Figure 5. Flowchart depicting our process for AER ST37 dataset cleaning and quality control.

A. Hosting, licensing, and maintenance plan

A.1. Hosting & Maintenance

We are hosting the dataset on Zenodo at : <https://zenodo.org/records/13743323>.

A.2. Data Licensing

The AWD Dataset is released under a Creative Commons Attribution-NonCommercial 4.0 International (CC BY-NC 4.0) License (<https://creativecommons.org/licenses/by-nc/4.0/>).

The satellite imagery for this project was acquired through Planet Labs' (PBC, 2024) Education & Research license, which allows the use of the data in publications and the creation of derivative products related to those publications. However, the raw imagery cannot be shared publicly. To adhere to these guidelines, we provide the data in HDF5 format, with the satellite imagery pre-processed to produce a derived product represented as a numpy array from Raster Vector. This process removes all geographic metadata.

This data is for academic use only and should not be used commercially. Proper credit to the current authors, Planet Labs (PBC, 2024), and the Alberta Energy Regulator (AER, 2024) is required when using this data.

B. Dataset Information

The purpose of this dataset is to assist in training deep learning systems to identify oil and gas wells, including abandoned, suspended, and active ones. This will enable the detection of wells in a specific area, allowing comparison with government records. If discrepancies are found, experts can conduct further investigations, which can possibly lead to the discovery of an abandoned or suspended device that might not be present in government records.

B.1. Dataset Structure

We provide training, validation, and testing sets, split using our proposed algorithm (as described in Section 3.2 of the main paper) to create a well-distributed dataset. The proposed method aims to create smaller regions of well concentration by clustering the centroids of patches. These regions are designed to be (a) mutually non-intersecting, (b) part of a larger geographic region by clustering the centroids of the initial clusters, and (c) containing a similar distribution of non-well patches within the same region.

This approach ensures that the training, validation, and test sets include representations from all geographic regions, providing a diverse and comprehensive evaluation. Thus, the dataset represents various geographical regions and offers a diverse benchmark for evaluation and testing. Each dataset split is saved in an HDF5 format file, structured as described in the following sections, and then compressed into a .tar.gz file for faster transfer.

Details on the number of samples in each set and the size of the dataset, both original and compressed, are presented in Table 3.

B.2. Dataset File Directory Structure

The following directory structure is used for each dataset file being stored in a Hierarchical Data Format 5 (HDF5) file:

```
<Train/Test/Val>Set.h5
  |---image
    |---<sample_name>
      |---Satellite Image (Multispectral Rasterio Image Data)
      |---Meta Data of <sample_name>
  |---label
    |---binary_seg_maps
      |---<sample_name>
        |---Binary Segmentation Map (Rasterio Image Data)
    |---multi_class_seg_maps
      |---<sample_name>
        |---Multiclass Segmentation Map (Rasterio Image Data)
  |---bounding_box_annotations
    |---<sample_name>
      |---Bounding Box JSON Data (COCO Format)
  |---author:Anonymous Author(s)
  |---description: Alberta Wells Dataset: Pinpointing Oil and Gas Wells
                  from Satellite Imagery
```

B.3. Structure of Dataset Directory

To enhance the efficiency of the data loader, we split the larger .h5 dataset into smaller .h5 files, each corresponding to a unique sample (image patch). By splitting the dataset in such a manner, we are able to improve the speed per iteration of the dataloader by over 100%.

This results in the following data structure:

```
<Sample_Id>.h5
  |---image
    |---Satellite Image (Multispectral Rasterio Image Data)
    |---Meta Data
  |---label
    |---binary_seg_maps
      |---Binary Segmentation Map (Rasterio Image Data)
    |---multi_class_seg_maps
      |---Multiclass Segmentation Map (Rasterio Image Data)
    |---bounding_box_annotations
      |---Bounding Box JSON Data (COCO Format)
  |---author:Anonymous Author(s)
  |---description: Alberta Wells Dataset: Pinpointing Oil and Gas Wells
                  from Satellite Imagery
```

B.4. Dataset Size & Distribution of Samples

Our dataset comprises over 94,000 patches of satellite imagery containing wells, with a total of 188,000 patches sourced from Planet Labs (PBC, 2024), covering more than 213,000 individual wells. Details about the distribution of the number of patches, wells present, and dataset split sizes are provided in Table 9, with the distribution of the number of wells per sample being described in Table 10. We also include an equal number of images that contain no wells in each dataset split. The distribution of wells per sample, along with the corresponding number of wells and the breakdown of well types, is illustrated in Figure 7 and detailed in Tables 11, 12, and 13. The geographic distribution of wells in the dataset can be visualized in Figure 6.

Table 9. Dataset statistics represented across the various splits of the dataset.

Dataset Split	No of Samples	No of Wells in Split	Original HDF5 File Size (in Gb)	Compressed .tar.gz File Size (in Gb)
Train	167436	194231	322	100
Validation	9463	8243	19	5.7
Test	11789	10973	24	7.1
Total	188688	213447	365	112.8

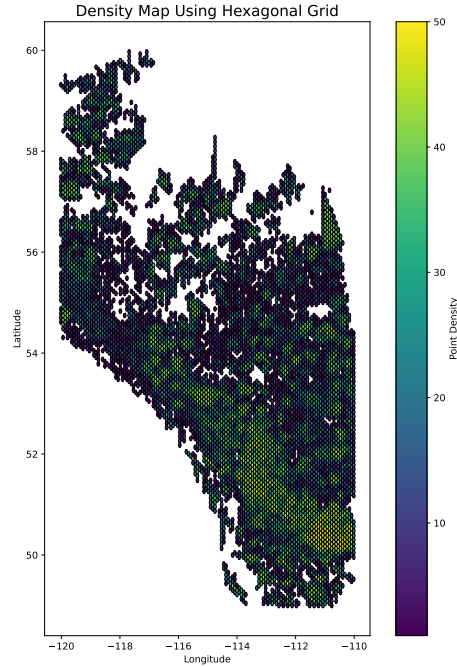
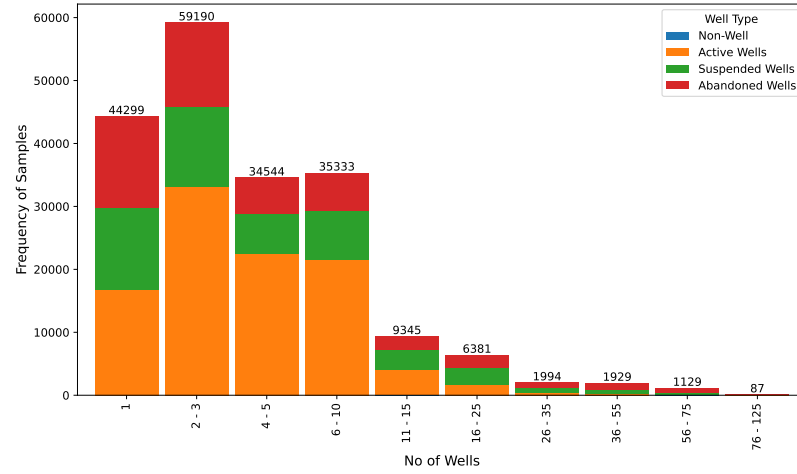


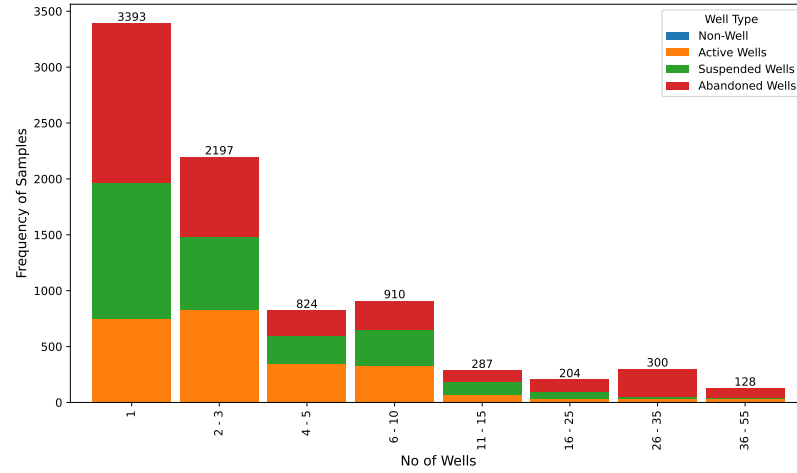
Figure 6. Density map of wells in the Alberta Wells Dataset.

Table 10. The distribution of individual wells in positive samples from the dataset. We also include an equal number of images that contain no wells in each dataset split.

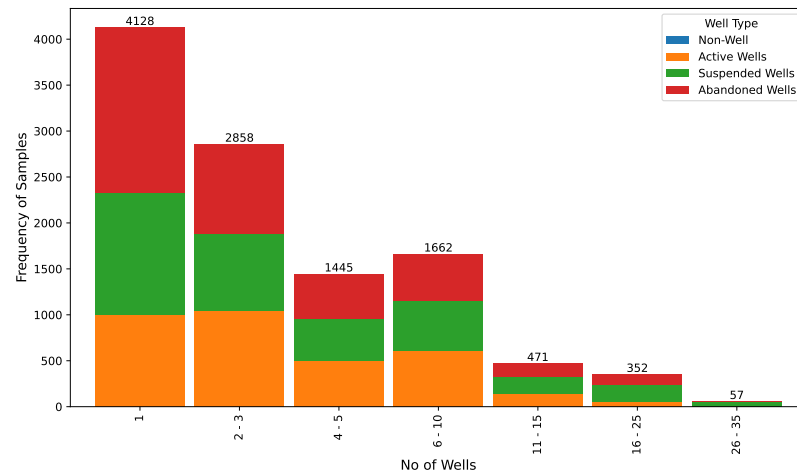
No of Wells in a Sample	Frequency of Well Instances in a Sample		
	Training Split	Validation Split	Test Split
1	44299	3393	4128
2 - 3	25378	979	1242
4 - 5	7899	190	328
6 - 10	4927	123	227
11 - 15	751	23	38
16 - 25	333	11	19
26 - 35	67	10	2
36 - 55	45	3	0
56 - 75	18	0	0
76 - 125	1	0	0
Total	83718	4732	5984



(a) Training set



(b) Validation set



(c) Test set

Figure 7. Distribution of the number of individual wells and the proportion of well types (active, suspended, and abandoned) in positive samples from the dataset. We also include an equal number of images with no wells at all.

Table 11. Test set statistics showing the distribution of image samples by the number of wells per image and the breakdown of well types (active, suspended, and abandoned).

No of Wells in a Image Sample (S)	Test Set				
	Count (Image Samples)	Distribution of Well Type in Samples			
		Total Wells	Active Wells	Suspended Wells	Abandoned Wells
1	4128	4128	999	1325	1804
2 - 3	1242	2858	1042	844	972
4 - 5	328	1445	495	464	486
6 - 10	227	1662	604	555	503
11 - 15	38	471	144	181	146
16 - 25	19	352	56	184	112
26 - 35	2	57	0	56	1
		10973	3340	3609	4024

Table 12. Validation Set statistics showing the distribution of image samples by the number of wells per image and the breakdown of well types (active, suspended, and abandoned).

No of Wells in a Image Sample (S)	Validation Set				
	Count (Image Samples)	Distribution of Well Type in Samples			
		Total Wells	Active Wells	Suspended Wells	Abandoned Wells
1	3393	3393	743	1225	1425
2 - 3	979	2197	833	654	710
4 - 5	190	824	346	248	230
6 - 10	123	910	323	331	256
11 - 15	23	287	67	114	106
16 - 25	11	204	32	63	109
26 - 35	10	300	33	22	245
36 - 55	3	128	29	14	85
		8243	2406	2671	3166

Table 13. Train Set statistics showing the distribution of image samples by the number of wells per image and the breakdown of well types (active, suspended, and abandoned).

No of Wells in a Image Sample (S)	Train Set				
	Count (Image Samples)	Distribution of Well Type in Samples			
		Total Wells	Active Wells	Suspended Wells	Abandoned Wells
1	44299	44299	16715	13116	14468
2 - 3	25378	59190	33099	12706	13385
4 - 5	7899	34544	22456	6321	5767
6 - 10	4927	35333	21522	7796	6015
11 - 15	751	9345	4076	3136	2133
16 - 25	333	6381	1781	2544	2056
26 - 35	67	1994	376	791	827
36 - 55	45	1929	172	777	980
56 - 75	18	1129	86	345	698
76 - 125	1	87	11	63	13
	83718	194231	100294	47595	46342

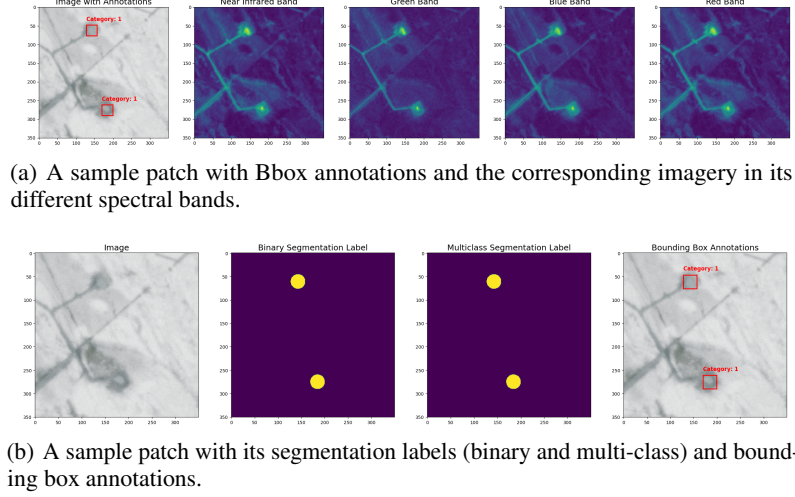


Figure 8. A Sample Patch from the Evaluation Set with 2 active wells.

B.5. PlanetScope Satellite Imagery

For our experiments, we selected a 4-band (RGBN) satellite imagery product (ortho_analytic_4b_sr) from Planet Labs (PBC, 2024) as illustrated in Figure 8. This product uses Planet’s PSB.SD instrument, which features a telescope with a larger 47-megapixel sensor and is designed to be interoperable with Sentinel-2 imagery in several bands. The frequency of each band of image is described in Table 14. The instrument provides a frame size of 32.5 km x 19.6 km, an image capture capacity of 200 million km²/day, and an imagery bit depth of 12-bit, with a ground sample distance (nadir) ranging from 3.7 m to 4.2 m.

The satellite images are corrected for atmospheric conditions and spectral response consistency. These multispectral products are tailored for monitoring in agriculture and forestry, offering precise geolocation and cartographic projection. They are ideal for tasks such as land cover classification, with radiometric corrections ensuring accurate data transformation.

Table 14. The Frequency of Each Spectral Band of a Planetscope PS.SD acquired Image

Band of Image	Frequency (in nm) of Spectral Band
Band 1 = Blue	465 - 515
Band 2 = Green	547 - 585
Band 3 = Red	650 - 680
Band 4 = Near-infrared	845 - 885

B.6. Meta Data Description

Each dataset sample is accompanied by metadata, including the sample name (sample ID in string format), the presence of a well in the sample, the number of wells in the sample, and whether a well of a specific category is present in the sample. Table 15 provides an illustration of metadata associated with a sample.

Table 15. Sample of Meta-Data Associated with each Instance in the Dataset

Meta-Data Attribute Name	Value
Sample_Name	eval_6934
wells_present	True
no_of_wells	10
Abandoned_well_present	True
Active_well_present	True
Suspended_well_present	True

B.7. Label Data Description

For our experiments, we create single-channel segmentation maps, which are binary maps used to locate instances of wells. We also generate multi-class segmentation maps, where each class denotes a well in an active, abandoned, or suspended state. Furthermore, we provide COCO format object detection labels for wells. In both segmentation and detection labels, we represent various states with class IDs as 'Active': 1, 'Suspended': 2, 'Abandoned': 3. To maintain consistency, we standardize the diameter of a well site to 90 meters (typically ranging from 70 to 120 meters) when annotating, resulting in a 30-pixel diameter in the labels. Figure 8(b) illustrates image patches with their corresponding labels, Figure 8(a) illustrates various spectral bands present in an image alongside the original image with bounding box annotations for reference and an example of a bounding box label in COCO format is shown below.

Sample of Bounding Box Annotation:

```
[
  {
    'id': 0,
    'image_id': 'eval_7028',
    'category_id': 1,
    'bbox': [46, 145, 29, 29],
    'iscrowd': 0
  },
  {
    'id': 1,
    'image_id': 'eval_7028',
    'category_id': 2,
    'bbox': [45, 127, 29, 29],
    'iscrowd': 0
  }
]
```

C. Dataset Samples Illustration

Samples from the dataset, covering various scenarios, are shown in Figures 9 and 10. A few more samples with prediction of the models and labels for binary segmentation and binary detection is illustrated in Figure 11.

D. Challenges for ML Community

The Alberta Wells Dataset presents several intriguing challenges for machine learning. Key issues include an imbalanced data distribution, with fewer instances of areas with multiple wells compared to those with single or two wells, and the visual similarity among active, suspended, and abandoned wells, which can confuse standard models. Additionally, varying spatial relationships in the imagery due to varying geography create difficulties for off-the-shelf models. Noise in annotations, even after data quality control and cleaning—such as misclassified wells—further complicates the task. Despite these challenges, the dataset's large scale and geographical diversity, covering over 213,000 wells, offer significant opportunities for developing robust and generalizable ML models for monitoring oil and gas infrastructure.

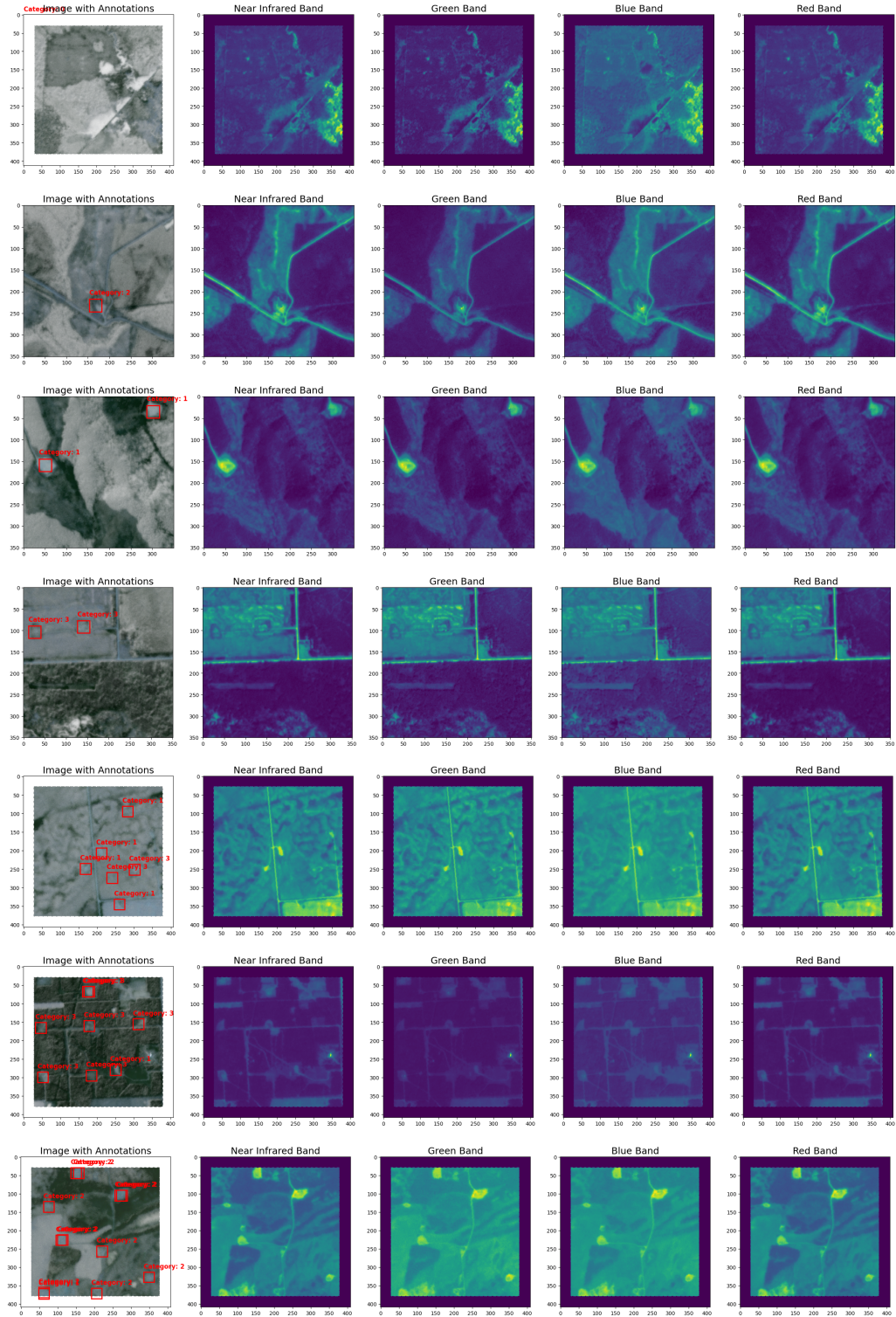


Figure 9. Qualitative results from the dataset illustrate the diverse distribution of wells in dataset samples, including Bbox annotations and corresponding imagery in different spectral bands.

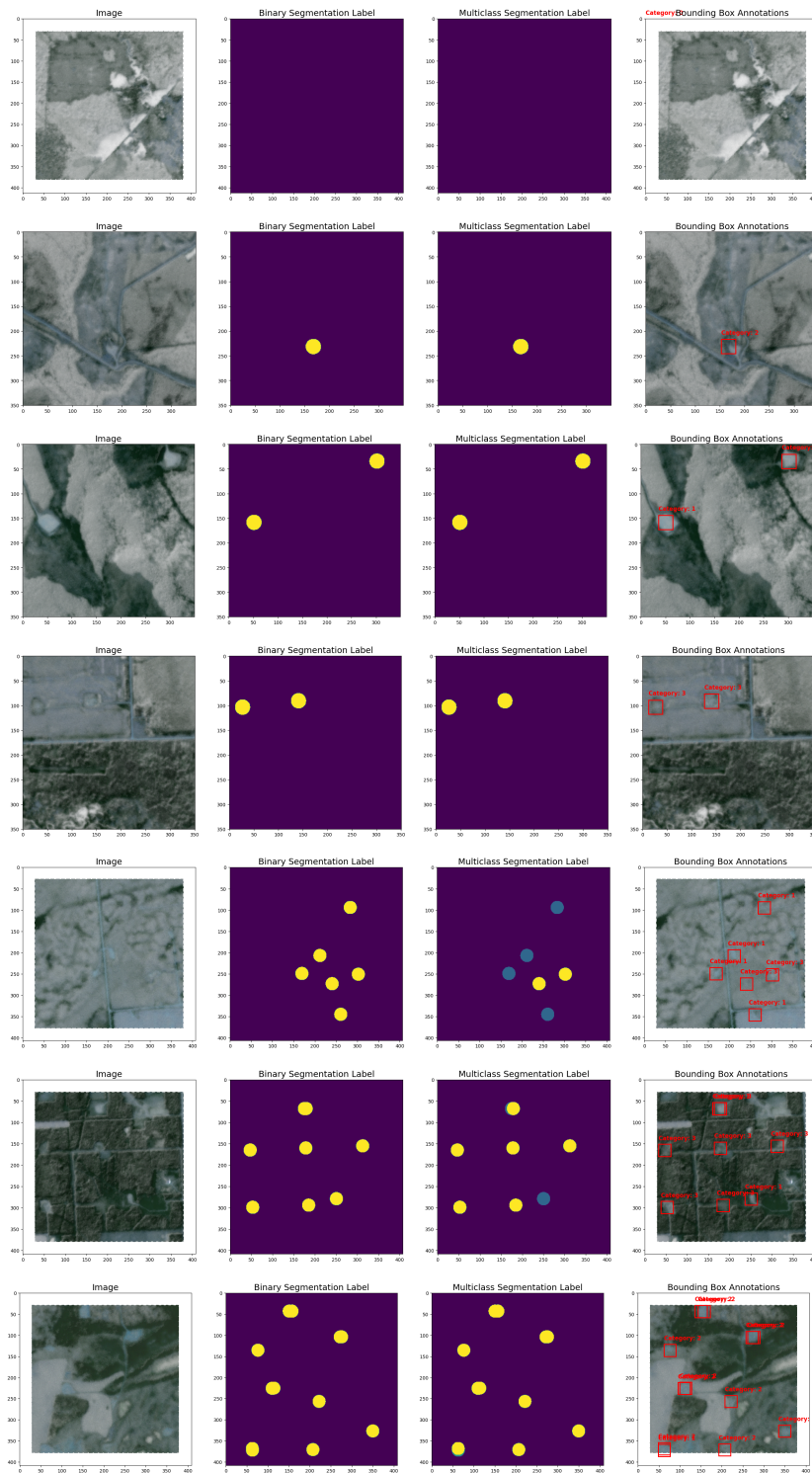


Figure 10. The qualitative results from the dataset showcase the varied distribution of wells in dataset samples, with their corresponding segmentation labels (binary and multi-class) and Bbox annotations.

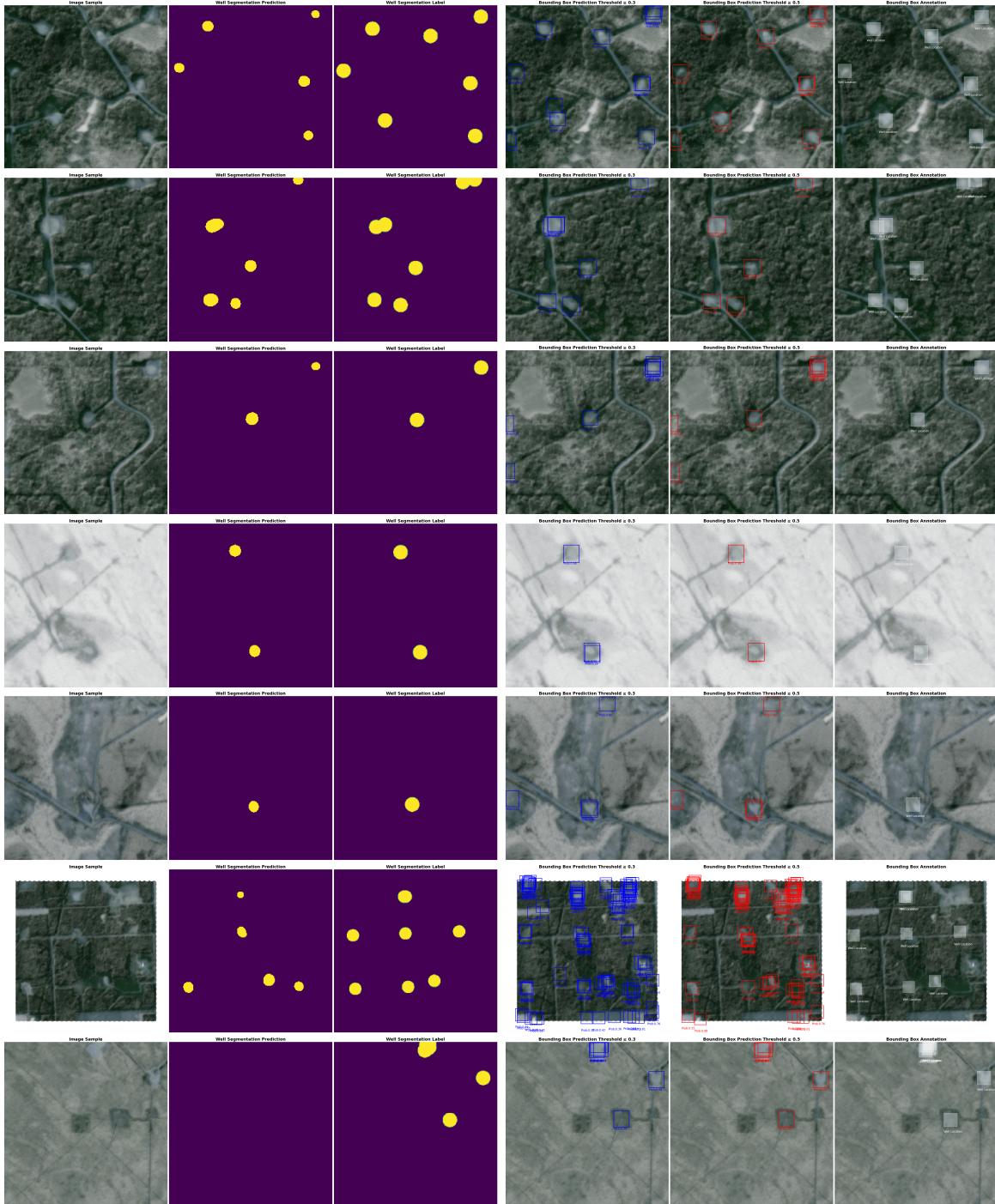


Figure 11. Few sample image patches from our dataset includes examples with no wells, two wells, and multiple wells. Additionally, we present qualitative results with predictions generated by our Segmentation U-Net (ResNet50) and DETR ResNet50 model.

E. Documentation frameworks: Datasheet for Datasets

E.1. Motivation

1. **For what purpose was the dataset created?** Was there a specific task in mind? Was there a specific gap that needed to be filled? Please provide a description.

The Alberta Wells Dataset (AWD) was created to identify oil and gas wells—whether abandoned, suspended, or active—using medium-resolution multi-spectral satellite imagery. While the issue of detecting oil and gas wells has been addressed by several authors, existing datasets are typically small (500-5,000 samples) and limited to specific regions, often including only active wells. This limitation reduces their effectiveness in identifying abandoned or suspended wells. The AWD aims to fill this gap in the literature by offering a comprehensive dataset with over 188,000 samples (including over 94,000 samples containing wells) from PlanetLabs satellite imagery, encompassing more than 213,000 individual wells.

2. **Who created the dataset (e.g., which team, research group) and on behalf of which entity (e.g., company, institution, organization)?**

The raw data is sourced from the Alberta Energy Regulator (AER), specifically from the monthly AER ST37 publication. This dataset includes comprehensive details about all reported wells in Alberta, such as their geographic location, mode of operation, license status, and the type of product extracted, among other attributes. The data is provided in shapefile format along with accompanying metadata. However, the dataset cannot be used directly because the license status or mode of operation often does not reflect the well's actual status. Therefore, the authors include domain experts, who specialize in field measurements of methane and air pollutant emissions from oil, gas, and urban systems, as well as in the geospatial and statistical data analysis of emissions and energy infrastructure, to ensure the quality of the dataset.

3. **Who funded the creation of the dataset?** If there is an associated grant, please provide the name of the grantor and the grant name and number.

This work was funded in part through the Canada CIFAR AI Chairs program and a McGill Tomlinson Scientist Award. We acknowledge support from Planet Labs in the form of their academic subscription program, and are grateful for the help of Tim Elrick in working with Planet data. We also thank Mila and the Digital Research Alliance of Canada for provision of computing facilities, and NVIDIA Corporation for additional computational resources.

E.2. Composition

- **What do the instances that comprise the dataset represent (e.g., documents, photos, people, countries)?** Are there multiple types of instances (e.g., movies, users, and ratings; people and interactions between them; nodes and edges)? Please provide a description.

We provide a dataset file stored in Hierarchical Data Format 5 (HDF5, i.e., a .h5 file), which contains multispectral 4-band RGBN satellite images in raster format and data labels with both identified by unique instance names. These satellite images, acquired from Planet Labs, have a resolution of 3 meters per pixel and include corresponding metadata. The metadata contains information about the number and types of wells present in a patch. For data labels, we offer binary segmentation maps, multi-class segmentation maps (each class representing a well in an active, abandoned, or suspended state), and COCO format object detection labels. The images were taken from the province of Alberta, Canada, with each satellite imagery patch representing a square with a side length of 1050 meters (1.05 km), covering an area of 1.025 square kilometers. The entire dataset spans over 193,000 square kilometers.

- **How many instances are there in total (of each type, if appropriate)?**

The proposed dataset comprises 188,688 instances, of which 94,344 contain one or more wells, totaling 213,447 well points. Each instance includes corresponding multispectral satellite imagery, segmentation maps (both binary and multi-class, with classes indicating active, suspended, or abandoned states), and bounding box annotations with the state of operations as the object class ID in COCO format. We standardized the diameter of a well site to 90 meters (typically ranging from 70 to 120 meters) for creating annotations, resulting in a diameter of 30 pixels in the labels. More details about the distribution of wells in each split are provided in the supplementary materials as well as the main paper.

- **Does the dataset contain all possible instances or is it a sample (not necessarily random) of instances from a larger set?** If the dataset is a sample, then what is the larger set? Is the sample representative of the larger set (e.g., geographic coverage)? If so, please describe how this representativeness was validated/verified. If it is not

representative of the larger set, please describe why not (e.g., to cover a more diverse range of instances because instances were withheld or unavailable).

The AWD Dataset is based on the AER ST37 monthly status data of wells in the Alberta region of Canada. It includes wells that are in active, suspended, or abandoned states of operation. To ensure the dataset’s quality, the authors with appropriate domain expertise conducted extensive quality control, filtering, and duplicate removal. This process was necessary because the full dataset included cases of well sites being restored and reclaimed, as well as various duplicates, noise, and data on other types of wells involving different natural resources. Therefore, the AWD Dataset, which includes multi-spectral satellite imagery, segmentation, and detection labels, is constructed from a refined subset of the original AER ST37 data, specifically targeting oil and gas wells that can be precisely identified.

- **What data does each instance consist of?** “Raw” data (e.g., unprocessed text or images) or features? In either case, please provide a description.

Each Image instance in our dataset, formatted in HDF5, contains satellite imagery represented as a numpy array from Raster Vector. We preprocessed this imagery by reprojecting it to the EPSG 32611 coordinate reference system and removed all geographic metadata, such as image bounds and coordinates, from the shared data. However, we do provide attributes like Sample Name, wells present, no of wells, Abandoned well present, Active well present, and Suspended well present. We utilized Planet Labs’ 4-band (RGBN) satellite imagery product (ortho_analytic_4b_sr), which incorporates the latest PSB.SD instrument with a 47-megapixel sensor. Each satellite imagery patch acquired represents a square with a side length of 1050 meters (1.05 km), covering an area of 1.025 square kilometers. The entire dataset spans over 193,000 square kilometers.

- **Is there a label or target associated with each instance?** If so, please provide a description.

There are three types of labeled data for each image: binary segmentation maps (in Rasterio Image format) indicating the presence or absence of oil and gas wells, multiclass segmentation maps (also in Rasterio Image format) potentially identifying various classes of objects, and bounding box annotations (in COCO format) specifying the location and size of objects, such as wells, within the image. These components together form a comprehensive dataset suitable for training and evaluating machine learning models for tasks like object detection and segmentation in satellite imagery, particularly focused on pinpointing oil and gas wells in Alberta

- **Is any information missing from individual instances?** If so, please provide a description, explaining why this information is missing (e.g., because it was unavailable). This does not include intentionally removed information but might include, e.g., redacted text.

The satellite imagery used in this project was obtained under Planet Labs’ (PBC, 2024) Education & Research license, which prohibits sharing raw satellite imagery. We re-projected the raw data to EPSG:32611 using the nearest resampling method and removed all geographic metadata, such as image bounds and coordinates, from the shared data imagery to create a derived product that complies with the license terms.

- **Are relationships between individual instances made explicit (e.g., users’ movie ratings, social network links)?** If so, please describe how these relationships are made explicit.

N/A

- **Are there recommended data splits (e.g., training, development/validation, testing)?** If so, please provide a description of these splits, explaining the rationale behind them.

The dataset we propose comprises more than 94,000 patches of satellite imagery containing wells, totaling 188,000 patches sourced from Planet Labs. This dataset covers over 213,000 individual wells. To ensure a balanced dataset, we divided it into training, validation, and testing sets using our algorithm outlined in Section 3.2 of the main paper. Our proposed method for splitting the data aims to create smaller, non-overlapping regions of concentrated wells by clustering patch centroids. These regions are intended to (a) not intersect, (b) be part of a larger geographic area by clustering initial cluster centroids, and (c) contain a similar distribution of non-well patches. This approach ensures that the training, validation, and test sets cover all geographic regions, providing a diverse and thorough evaluation. The dataset splits represent various geographical areas, making it a comprehensive benchmark for evaluation and testing. Each dataset split is stored in an HDF5 format file.

- **Are there any errors, sources of noise, or redundancies in the dataset?** If so, please provide a description.

One limitation of our study is our reliance on well locations provided by the Alberta Energy Regulator, which may not encompass all sites, leading to potential omissions in the ground-truth data. This could result in a lower reported validation and test accuracy, with some correctly predicted well locations being mistakenly categorized as false.

- **Is the dataset self-contained, or does it link to or otherwise rely on external resources (e.g., websites, tweets, other datasets)?** If it links to or relies on external resources, a) are there guarantees that they will exist and remain constant, over time; b) are there official archival versions of the complete dataset (i.e., including the external resources as they existed at the time the dataset was created); c) are there any restrictions (e.g., licenses, fees) associated with any of the external resources that might apply to a dataset consumer? Please provide descriptions of all external resources and any restrictions associated with them, as well as links or other access points, as appropriate.

The dataset does not rely on the persistence of external resources.

- **Does the dataset contain data that might be considered confidential (e.g., data that is protected by legal privilege or by doctor-patient confidentiality, data that includes the content of individuals' non-public communications)?** If so, please provide a description.

No.

- **Does the dataset contain data that, if viewed directly, might be offensive, insulting, threatening, or might otherwise cause anxiety?** If so, please describe why.

No.

E.3. Collection Process

- **How was the data associated with each instance acquired?** Was the data directly observable (e.g., raw text, movie ratings), reported by subjects (e.g., survey responses), or indirectly inferred/derived from other data (e.g., part-of-speech tags, model-based guesses for age or language)? If the data was indirectly inferred/derived from other data, was the data validated/verified? If so, please describe how.

The AER publishes AER ST37, a monthly list of wells in Alberta, including location, operation mode, license status, and product type. However, the data needs rigorous quality control as license status, or operation mode may not accurately reflect the actual well status. The authors, with extensive domain expertise, removed duplicate well entries in the metadata and shapefile, keeping the most recent update. We then merge and filter the datasets, categorizing wells as active, abandoned, or suspended based on expert criteria. Duplicate coordinates are resolved by keeping the instance with the latest drill date. We verify all wells are within Alberta's boundaries. After thorough quality control by domain experts, we calculate the geographical bounds covered by wells and divide the region into non-overlapping square patches. These patches include varying numbers of wells, with an equal number of patches with and without wells.

- **What mechanisms or procedures were used to collect the data (e.g., hardware apparatus or sensors, manual human curation, software programs, software APIs)?** How were these mechanisms or procedures validated?

We acquired multispectral satellite imagery data from Planet Labs, which comprises four bands (RGBN) with a 3-meter-per-pixel resolution obtained through their proprietary API. This data was processed using quality-controlled and cleaned well data to generate segmentation and object detection annotations. The annotations were created using custom Python code, leveraging libraries like Shapely, GeoPandas, and Rasterio, and were validated through visualization using folium and matplotlib.

- **If the dataset is a sample from a larger set, what was the sampling strategy (e.g., deterministic, probabilistic with specific sampling probabilities)?**

No.

- **Who was involved in the data collection process (e.g., students, crowdworkers, contractors) and how were they compensated (e.g., how much were crowdworkers paid)?**

The dataset was a collaborative effort involving the Alberta Energy Regulator, Planet Labs, and the authors. Without the contributions from individuals in these three organizations, this dataset would not have been possible. Proper credit must be given to the authors, Planet Labs, and the Alberta Energy Regulator when using this data.

- **Over what timeframe was the data collected?** Does this timeframe match the creation timeframe of the data associated with the instances (e.g., recent crawl of old news articles)? If not, please describe the timeframe in which the data associated with the instances was created.

We acquired the data from the Alberta Energy Regulator, specifically from its monthly well bulletin AER ST37 (AER, 2024), dated March 2024. Leveraging domain expertise, we filtered the data to reflect the condition of wells as of September 30, 2023. This decision was made because imagery acquired from Alberta during the winter months tends

to have high cloud cover. Therefore, we filtered the data to ensure we could collect the best data for each patch based on satellite data acquired between the summer months of June and September in the region.

- **Were any ethical review processes conducted (e.g., by an institutional review board)?** If so, please provide a description of these review processes, including the outcomes, as well as a link or other access point to any supporting documentation.

N/A

E.4. Preprocessing/cleaning/labeling

- **Was any preprocessing/cleaning/labeling of the data done (e.g., discretization or bucketing, tokenization, part-of-speech tagging, SIFT feature extraction, removal of instances, processing of missing values)?** If so, please provide a description.

In the Dataset section of our submission, we provide a detailed description of the quality control, cleaning, and labeling processes applied to the data obtained from the Alberta Energy Regulator, which forms the basis of our dataset. The satellite imagery utilized in this project was acquired under the Education & Research license from Planet Labs. We reprojected the raw data to EPSG:32611 using the nearest resampling method. Additionally, we removed all geographic metadata, such as image bounds and coordinates, from the shared data imagery to ensure compliance.

- **Was the “raw” data saved in addition to the preprocessed/cleaned/labeled data (e.g., to support unanticipated future uses)?** If so, please provide a link or other access point to the “raw” data.

The raw satellite imagery data has been saved for internal use; however, it cannot be shared in its current form. Before sharing, the data must undergo preprocessing to remove metadata, as stipulated by the agreement mentioned earlier.

- **Is the software that was used to preprocess/clean/label the data available?** If so, please provide a link or other access point.

We plan to share the relevant code used for dataset quality control, patch creation, dataset splitting, data acquisition, and label and HDF5 file creation with the public release of the dataset in the future.

- **Any other comments?**

N/A

E.5. Uses

- **Has the dataset been used for any tasks already?** If so, please provide a description.

Currently, there are no public demonstrations of the AWD Dataset in use. In this work, we showcase its application for Binary Segmentation and Binary Object Detection of Well Sites to train algorithms for accurately locating well sites. These algorithms can be scaled across larger regions of interest to compare against existing databases, identifying potentially undocumented wells. Flagging wells not present in databases is crucial, as these could be abandoned wells that are significant emitters of greenhouse gases, making them candidates for plugging.

- **Is there a repository that links to any or all papers or systems that use the dataset?** If so, please provide a link or other access point.

N/A

- **What (other) tasks could the dataset be used for?**

Additionally, we provide multi-class labels indicating the operational state of the wells for both cases. These labels can be utilized in future projects for locating wells and classifying their operational status, which will aid in identifying well sites that are not present in government records.

- **Is there anything about the composition of the dataset or the way it was collected and preprocessed/cleaned/labeled that might impact future uses?**

This dataset focuses on Alberta, Canada, known for its diverse oil reserves and varied landscapes, providing a representative sample comparable to regions in the Appalachian and Mountain West areas of the United States and some former Soviet states with oil wells and unidentified site issues. A limitation of our study is the reliance on well locations from the Alberta Energy Regulator, which may miss some sites, leading to potential false negatives in the ground-truth data. However, this should have minimal impact on algorithm training, as these labels are a minor part of the dataset, and

deep learning algorithms can handle moderate label noise well (see e.g., (Rolnick et al., 2017)). The main effect may be underreported test accuracy, with some correctly predicted well locations wrongly counted as false. We plan to investigate this further in future work. Additionally, the use of multi-spectral optical data in the AWD dataset may limit the models' applicability in regions with frequent cloud cover.

- **Are there tasks for which the dataset should not be used?** If so, please provide a description.
This dataset is intended for non-commercial use only and should not be utilized in any application that could negatively impact biodiversity.
- **Any other comments?**
N/A

E.6. Distribution

- **Will the dataset be distributed to third parties outside of the entity (e.g., company, institution, organization) on behalf of which the dataset was created?** If so, please provide a description.
Yes, the dataset will be made public (open-source) in the future.
- **How will the dataset will be distributed (e.g., tarball on website, API, GitHub)?** Does the dataset have a digital object identifier (DOI)?
The dataset is accessible through Zenodo.
- **When will the dataset be distributed?**
The Dataset is made public and hosted on Zenodo at <https://zenodo.org/records/13743323>.
- **Will the dataset be distributed under a copyright or other intellectual property (IP) license, and/or under applicable terms of use (ToU)?** If so, please describe this license and/or ToU, and provide a link or other access point to, or otherwise reproduce, any relevant licensing terms or ToU, as well as any fees associated with these restrictions.
The AWD Dataset is released under a Creative Commons Attribution-NonCommercial 4.0 International (CC BY-NC 4.0) License (<https://creativecommons.org/licenses/by-nc/4.0/>).
- **Have any third parties imposed IP-based or other restrictions on the data associated with the instances?** If so, please describe these restrictions and provide a link or other access point to, or otherwise reproduce, any relevant licensing terms, as well as any fees associated with these restrictions.
The satellite imagery used in this project was acquired under the Education & Research license of Planet Labs (PBC, 2024). This license allows for the use of the data in publications and the creation of derivative products, which can be shared in association with publications. However, raw imagery cannot be shared publicly. To comply with these guidelines, we share the data in HDF5 format, with satellite imagery represented as a numpy array from Raster Vector. We have removed all geographic metadata, such as image bounds and coordinates, from the shared data. The data is intended for academic use only and should not be used for commercial purposes. Proper credit must be given to the current authors, Planet Labs, and the Alberta Energy Regulator when using this data.
- **Do any export controls or other regulatory restrictions apply to the dataset or to individual instances?** If so, please describe these restrictions, and provide a link or other access point to, or otherwise reproduce, any supporting documentation.
No
- **Any other comments?**
N/A

E.7. Maintenance

- **Who is supporting/hosting/maintaining the dataset?**
The dataset is hosted on Zenodo.
- **How can the owner/curator/manager of the dataset be contacted (e.g., email address)?**
You can reach the authors through the email addresses provided in the paper. Additionally, you can raise any issues on the GitHub repository, which will be made public in the future.

- **Is there an erratum?** If so, please provide a link or other access point.
Not to the best of our knowledge.
- **Will the dataset be updated (e.g., to correct labeling errors, add new instances, delete instances)?** If so, please describe how often, by whom, and how updates will be communicated to users (e.g., mailing list, GitHub)?
As our dataset is based on data from a fixed timeframe and consists of satellite imagery collected during a specific period, we do not currently have plans to update it in the near future. However, if there are any changes to these plans, updates to the dataset will be posted on the corresponding GitHub repository once it is made public.
- **Will older versions of the dataset continue to be supported/hosted/maintained?** If so, please describe how. If not, please describe how its obsolescence will be communicated to users.
If there are newer versions of the dataset, they will maintain the same format. We will ensure that the code associated with the project on GitHub supports these updates, and we will update the READMEs to reflect any changes to the dataset.
- **If others want to extend/augment/build on/contribute to the dataset, is there a mechanism for them to do so?** If so, please provide a description. Will these contributions be validated/verified? If so, please describe how. If not, why not? Is there a process for communicating/distributing these contributions to users? If so, please provide a description. We plan to share the relevant code in the future. However, to ensure the ability to compare against our results, we encourage those who wish to build on the dataset to publish their work separately rather than adding to our data repository.
- **Any other comments?**
N/A